Report No. 82
DOE/ET/52008-1
UC-20 c

Columbia University
in the City of New York

THE INTERACTION OF GRAPHITE WITH A HOT, DENSE DEUTERIUM PLASMA

JOHN C. DESKO, JR.

1980

Work Supported by DOE Contract DE-AS02-77ET52008

Plasma Laboratory
School of Engineering and Applied Science
Columbia University
New York, N.Y. 10027

DISCLAIMER

Master

Report No. 82
DOE/ET/52008-1
UC-20 c

THE INTERACTION OF GRAPHITE WITH A HOT, DENSE DEUTERIUM PLASMA

JOHN C. DESKO, JR.

1980

Work Supported by DOE Contract DE-AS02-77ET52008

Plasma Laboratory
School of Engineering and Applied Science
Columbia University
New York, N.Y. 10027

ABSTRACT

THE INTERACTION OF GRAPHITE
WITH A HOT,
DENSE DEUTERIUM PLASMA

JOHN C. DESKO, JR.

The first wall of future fusion reactors will be subjected to intense bombardment by neutrons, electrons, and energetic ions. The ability of various materials to perform successfully over long periods of exposure is a timely research topic. Graphite is being considered for use as a fusion reactor component (limiters, beam dumps, etc.) because carbon impurities radiate significantly less energy, which is lost from the fusion process, than all other higher atomic number impurities.

The erosion of ATJ-S graphite caused by a hot, dense deuterium plasma has been investigated experimentally. The plasma was produced in an electromagnetic shock tube. Plasma characteristics were typically: ion temperature $\simeq$ 800 eV ($\sim 1 \times 10^7$ ^{o}K), number density $\simeq 10^{16}/cm^3$, and transverse magnetic field $\simeq$ 1 tesla. The energetic ion flux, ϕ, to the sample surfaces was $\sim 10^{23}$ ions/cm^2-sec for a single pulse

duration of $\sim$ 0.1 usec. Sample surfaces were metallographically prepared and examined with a scanning electron microscope before and after exposure.

Samples of ATJ-S graphite were subjected to as many as 200 pulses. Surface erosion was found and was observed to increase linearly with exposure. Erosion was not uniform over the surface. Significantly greater erosion was observed in the thin regions above sub-surface pores. Considerable flaking was observed in these regions and is attributed to stresses arising from the thermal expansion of the surrounding material. However, no cracking or other serious structural damage was observed.

After the graphite had been exposed to the hot, dense deuterium plasma, the residual gas was analyzed for evidence of the formation of volatile hydrocarbons resulting from the erosion of the graphite surfaces by the plasma. CD_4 was clearly observed as an erosion product. The impurity production rate for ATJ-S graphite was calculated and found to be 18 ± 12 carbon atoms/incident deuterium ion. This indicates that erosion is not due to such classical erosion mechanisms as physical and chemical sputtering. Erosion is attributed to arcing and sublimation.

These studies indicate that ATJ-S graphite is a superior material, with regard to the maintenance of structural integrity, for use in a fusion reactor. However, the

high impurity production rate places an upper limit on the amount of graphite that can be exposed to plasma bombardment in a fusion reactor.

TABLE OF CONTENTS

ACKNOWLEDGEMENTS

The author wishes to express his deepest gratitude to all who helped make this a successful effort. I thank Dr. John Tien, my advisor, for his encouragement and guidance. I also thank Dr. Robert Gross for his enthusiasm and advice. I am grateful to Mr. Maurice Cea, Mr. George Senko, Mr. John Osarczuk, and Mr. William O'Connor for their technical assistance at various stages of this project. I am especially grateful to Mr. Robert Jarrett for his valuable assistance, suggestions, and discussions and especially for his friendship. I am also very grateful to Mr. William Botjer, my friend, for his invaluable moral support. I am very thankful to my parents for their love, encouragement, and support throughout my entire life. Finally, I am most thankful to my wife, Linda, for her love, support, counsel, encouragement, enthusiasm, understanding, and humor.

I. INTRODUCTION

It is known that plasma-wall interactions are of critical importance in the operation of a tokamak fusion power reactor.[1-3] Small amounts of wall material ejected into the deuterium plasma through such processes as physical sputtering[1-4], chemical sputtering[1,3], unipolar arcing[1,3], and thermal evaporation[1,3], can result in significant energy loss by bremsstrahlung radiation. Such loss can prevent fusion ignition.[5,6,7]

Low atomic number impurity atoms radiate significantly less energy than high atomic number impurity atoms since bremsstrahlung radiation is directly proportional to Z^3, where Z is the atomic number of the impurity.[6,7,8] Consequently, wall materials with low atomic number have been suggested for use in plasma environments, especially at such sites as limiters and beam dumps where wall loading is the most severe. One material which is receiving considerable attention is graphite with a Z of 6.

The advantage of using a low-Z material such as graphite is negated, however, if the production rate of impurity atoms is excessive.[6,7] Hence, to correctly evaluate the merits of graphite as a candidate fusion reactor component material, the impurity production rate must be determined under conditions expected to be found in the antici-

pated fusion reactor.

The impurity production rate and dominant erosion mechanisms have not yet been determined for the high incident fluxes of energetic ions (10^{22}-10^{23} ions/cm^2-sec) which are expected to exist in certain areas of the anticipated fusion reactor such as, again, limiters and beam dumps.[9,10] It is precisely in these areas of higher flux that the use of graphite appears most attractive due to the high sublimation temperature (3350^{o}C) of graphite which allows it to sustain a considerable level of heat loading.

Very little quantitative information exists on the erosion of ATJ-S graphite. This type of bulk graphite is expected to be used in a fusion reactor because of its exceptional thermal shock resistance characteristics. ATJ-S graphite is a molded, fine grain graphite with a density of $\sim$1.85-1.90 grams/cm^3 and a pore volume of $\sim$ 18%.[11]

Most previous erosion results were obtained at much lower incident particle flux ranges (10^{14}-10^{18} ions/cm^2-sec) and on pyrolytic graphite instead of ATJ-S graphite.[12-27] Pyrolytic graphite has a high degree of directional crystallinity and is formed by vapor deposition in thin layers, and hence, is not as suitable for use as bulk components in the fusion reactors. In these studies[12-27], chemical sputtering was found to be the dominant erosion and impurity production mechanism above ambient temperature with CD_4 (CH_4)

being the reaction product. The temperature of maximum impurity production was found to occur at about 570°C. For bombardment by energetic ions (100 eV $\leqslant$ E $\leqslant$ 10 keV), the chemical sputtering rate was found to be between 2.5×10^{-2} and 1.0×10^{-1} molecules/incident ion. These experiments were performed using ion beams which precluded the occurrence of arcing, an erosion mechanism which requires the presence of both ions and electrons. However, recent qualitative results on the erosion of graphite limiters by a plasma (ions and electrons) indicate that arcing may be the dominant erosion mechanism for graphite under tokamak conditions.[11,28,29]

In this thesis, the erosion of ATJ-S graphite by a hot, dense deuterium plasma has been investigated experimentally at an incident particle flux of $\sim 10^{23}$ ions/cm^2-sec. The plasma was produced by an electromagnetic shock tube which has been used previously in similar studies involving the interaction of deuterium plasma with metals and alloys.[30] After exposure of the graphite samples to the plasma, the residual gas was analyzed using a monopole gas analyzer to identify volatile hydrocarbons resulting from the interaction of the deuterium ions with the graphite surface and to evaluate the impurity production rate for hydrocarbon formation. Specimen surfaces were also examined after exposure to identify the damage modes and to discern trends in surface damage.

II. REVIEW OF PREVIOUS WORK

The deuterium particle flux presently anticipated in an operating tokamak is $\sim 10^{12}$-10^{13} particles/cm^2-sec at the wall and $\sim 10^{22}$-10^{23} particles/cm^2-sec at the limiters. The anticipated tokamak pulse length is $\sim 10^2$-10^4 sec. The average energy of an incident deuterium particle will be $\sim$10-300 eV at the walls and $\sim$100-1000 eV or higher at the limiter and the average wall and limiter temperature is expected to be $\sim 500^{\circ}$C.[28,29] The interaction of such a hot, dense plasma with wall materials results in the introduction of impurity atoms into the plasma from the wall primarily through such mechanisms as physical sputtering, chemical sputtering, and arcing.

Physical sputtering is a momentum transfer process between the incident deuterium ions and the wall atoms. Upon collision, a deuterium ion transfers momentum to the wall by a cascade collision and a wall atom near the point of impact leaves the surface after gaining sufficient energy to break its surface bonds. Physical sputtering theory[1,2,3,4] is well established for the sputtering of high-Z wall atoms; however, the application of the theory to low-Z wall atoms such as carbon is questionable. This is primarily due to the assumptions made in the model. The theory does indicate that physical sputtering is virtually independent of temper-

ature below .8 Tm, where Tm is the melting point, for all materials.[4]

Chemical sputtering[1,3] is a mechanism whereby the incident deuterium ions react chemically with the wall to form volatile molecules which are loosely bound to the wall and are subsequently released into the plasma. This mechanism is confined to those materials which form volatile molecules with deuterium; whereas, physical sputtering occurs for all materials to varying degrees. Since chemical sputtering involves chemical reactions, it is expected to be extremely temperature dependent and very material dependent.

Arcing[1,3] is a mechanism whereby an intense electric current channel is formed between the wall and the plasma. Arcing is thought to be due to the known formation of an electric sheath potential at the wall-plasma interface. The sheath results from the increased flux of electrons from the plasma. Localized surface heating and melting allows positive ions and neutrals to leave the wall and enter the plasma. However, very little is known about the mechanisms of arc initiation or the impurity production rate from arc erosion.

The introduction of impurities into the plasma through mechanisms previously mentioned is cause for serious concern. Impurities can result in significant energy loss by radiation from the plasma such that the attainment of fu-

sion ignition is impossible. Radiation loss occurs through bremsstrahlung radiation and is proportional to $N_e \sum N_j Z_j^2$ where N_e is the electron concentration, Z_j is the atomic number of the j^{th} impurity species, and N_j is the ion concentration of the j^{th} impurity species. The summation is carried out over all the impurity species present in the plasma.

To determine the severity of this problem, it is necessary to consider the effect of plasma impurities on Lawson's criteria.[5,6,7] This criteria states that for a fusion reactor to produce more energy than is needed to heat the plasma, the product of the plasma density, n, and the plasma energy confinement time, t, must be equal to or greater than a calculated value. This value depends on the plasma temperature, T, and is determined from energy balance equations which take into account all plasma energy loss mechanisms. For plasma temperatures of 10 keV and 20 keV, the minimum values of nt are $\sim 4 \times 10^{20}$ sec/m^3 and $\sim 1.5 \times 10^{20}$ sec/m^3, respectively, for a plasma containing equal parts of deuterium and tritium and no impurities.[6,7]

The effect of plasma impurities on Lawson's criteria is shown for several different impurities in Figure 1. The shapes of the curves and the relative positions of the curves are determined to a large degree by the bremsstrahlung radiation loss term. It is seen that the minimum value

of nt increases rapidly and there exists a critical impurity concentration for each impurity specie above which, net fusion power is impossible. These critical concentrations are shown in Figure 2 for several impurities.

The effect of impurities upon Lawson's criteria is seen to be substantial. Since an increase in nt results in a significant increase in the amount of energy needed for plasma heating, it is imperative to not only keep impurity concentrations below the critical values, but to try to keep nt as near as possible to the minimum value by reducing impurity concentrations to the lowest possible value.

Numerous investigations[11-29] have been undertaken to experimentally determine the impurity production rate of graphite under deuterium or hydrogen bombardment to evaluate graphite's usefulness as a tokamak fusion reactor material. These investigations involved bombardment by either beams of ions[13,14,16-27] or plasmas.[11,12,15,28,29] Ion beam experiments, because of the inherent absence of electrons, give no information on arcing or its seriousness as an erosion mechanism. Experiments utilizing ion beams are limited to the study of such classical erosion mechanisms as physical or chemical sputtering, in which electrons do not play a role.

The interaction of thermal deuterium (hydrogen) atoms or ions with graphite has been experimentally studied by several authors using either ion beams[13,14,16] or

plasmas[12,15] produced by a radio frequency voltage. The impurity production rate was determined by either mass spectroscopy of the residual gas or weight change measurements of the graphite samples. The rate was found to be very temperature dependent and the maximum value ranged between 4 x 10^{-5} atoms/ion and 4.5 x 10^{-3} atoms/ion and occurred in the material temperature range of 400°C to 630°C. Impurity production is attributed primarily to the chemical sputtering of the graphite with CD_4 (CH_4) as the principal chemical sputtering product below 800°C. Above 800°C, C_2D_2 (C_2H_2) has also been identified as a chemical sputtering product by Balooch and Olander.[14] Wood and Wise[12] and McCracken and Patridge[15] also report the occurrence of hydrocarbon molecules with two or more carbon atoms as erosion products. However, there is some question as to whether these hydrocarbon molecules actually resulted from the erosion of graphite or rather from some other chemical process.

Several authors[17-27] have also studied the interaction of energetic deuterium (hydrogen) ions with graphite using ion beams. The ion energies used in these experiments ranged between 100 eV and 30 keV. In these experiments, the impurity production rate was determined by either mass spectroscopy, height or weight change measurements, or auger electron spectroscopy. The rate was found to be very temperature dependent. Values of the impurity production rate

at room temperature varied between 2.4 x 10^{-3} atoms/ion and 5 x 10^{-2} atoms/ion. Maximum values of the impurity production rate varied between 2.5 x 10^{-2} atoms/ion and 1.0 x 10^{-1} atoms/ion and occurred in the material temperature range of 530°C to 650°C. Impurity production at room temperature is attributed solely to the physical sputtering of carbon atoms from the graphite surface. The increase in impurity production at higher temperatures is attributed to chemical sputtering. CD_4 (CH_4) is the only identified chemical sputtering product.

A summary of the results for both thermal and energetic, atoms and ions is shown in Table 1. The chemical sputtering rates for energetic ions are almost two to three orders of magnitude higher than for those for thermal atoms and ions. The higher rates are probably due to the higher trapping efficiency of the energetic ions as compared with the low sticking efficiency of the thermal atoms and ions.[1] The energetic ion data is more applicable to fusion reactor materials studies since the incident ion energy is in the range of that expected for the anticipated fusion reactor.

Braganza et. al.[24] has suggested a model of chemical sputtering by energetic ions where the ion-induced desorption of deuterium from the surface layer of graphite is the critical variable in chemical sputtering yield. The model predicts that the erosion rate should decrease and the tem-

perature of maximum chemical sputtering should increase with increasing particle flux. In addition, it predicts that the chemical sputtering rate is only weakly dependent upon particle energy. All of these points are supported by the authors' experimental data.

Smith and Meyer[27] have shown that the apparent scatter in chemical sputtering rate results of six authors[17,19-22,27] could be successfully explained by the model of chemical sputtering developed by Braganza et. al.[24] in which the incident particle flux, which varied from one investigation to another, and ranged from 10^{14} to 10^{18} ions/cm^2-sec, is taken into account. However, the authors' corrections to the data of Feinberg and Post[17] do not seem justified and hence agreement between theory and experiment at a particle flux of 10^{18} ions/cm^2-sec or greater is questionable.

Several authors[11,28,29] have studied the erosion of graphite limiters by a plasma in experimental tokamaks. In all of these experiments, the partial pressure of CD_4 was found to increase after plasma bombardment. Arcing damage was evident on the limiter surfaces exposed to the plasma and was reported as the primary erosion mechanism.[11,28] The impurity production rates were not reported, however, since these experiments were qualitative in nature.

To correctly evaluate the usefulness of ATJ-S graphite as a fusion reactor material, the impurity production

rate of ATJ-S graphite must be determined under conditions expected to exist in an operating fusion power plant. A review of previous works, summarized in Table 1, shows that this has not been done. The impurity production rate has been determined for particle fluxes that are many orders of magnitude lower than that expected to exist at the limiters and beam dumps of tokamak reactors. In addition, these studies have been confined to pyrolytic graphites which are considerably different from ATJ-S graphite. Finally, these results were obtained using ion beams which precluded the occurrence of arcing. Results obtained on the erosion of graphite limiters by a plasma indicate that arcing may be the most serious erosion and impurity production mechanism for graphite under plasma bombardment. If this is the case, then the impurity production rate for graphite under plasma bombardment may be quite different from that obtained in ion beam experiments.

III. EXPERIMENTAL PROCEDURE

A. Equipment

Shock Tube

The Columbia University Electromagnetic Shock Tube is a pulsed device that produces a plasma by shock wave heating and compression.[31] It has been used previously for plasma-wall interaction studies involving metals and alloys and is described in detail in reference 30.

Briefly, the shock tube consists of two concentric cylinders of length 1.8 m and diameters 23 cm and 13 cm. A rod, electrically insulated from the cylinders is located on the axis of the cylinders. The cylinders and rod are made of OFHC copper. The plasma is formed in the annulus between the cylinders. The shock tube is shown schematically in Figure 3.

The plasma is produced by first evacuating the annulus region to a base pressure of less than 1.3×10^{-4} Pa and then filling this region with deuterium gas to a pressure of 6.7 Pa. A slow rise time ($\sim$ 50 usec) capacitor bank is then discharged through the bias rod producing a transverse magnetic field. When this field is approximately constant, a fast rise time ($\sim$5 usec) capacitor bank is discharged between the inner and outer conducting cylinders, forming a radial current sheet at one end of the tube, the launching

wall. This current sheet interacts with the transverse magnetic field resulting in a $\vec{J} \times \vec{B}$ force which propels the plasma along the tube axis from the launching wall and toward the reflecting end wall. After shock reflection at the end wall, the plasma comes to rest in the vicinity of the end wall.

Six ports are situated on the outer conductor near the end wall. They allow samples of 6 mm diameter to be inserted into the shock tube for the irradiation of the sample surfaces. The ports contain valves which allow for easy insertion and removal of the samples.

Plasma conditions in this sample region have been well documented by previous investigators.[32-36] Plasma characteristics are listed in Table 2. Thus for each pulse of the shock tube, each sample is bombarded by $\sim 10^{16}$ ions/cm^2.

Residual Gas Analyzer

A residual gas analyzer was used to analyze the shock tube gas for evidence of hydrocarbon molecules resulting from the erosion of graphite and to determine the impurity production rate for hydrocarbon production. The gas analyzer was a Veeco model SPI-10 monopole gas analyzer.

The analyzer's functions are described in detail in its operation manual. Briefly, gas molecules enter the analyzer tube and are ionized by high energy electrons emitted from a heated filament. The ionized molecules are then ac-

celerated into the analyzing region which consists of a V-shaped rail and a cylindrical rod positioned parallel to and a precise distance apart from the rail. The rod is supplied with a radio frequency voltage superimposed on a direct current voltage. Ionized molecules entering this region oscillate in a complex fashion. For particular electrical conditions, only ionized molecules of a specific mass-to-charge ratio will move in a path which results in their impingement upon a collector. Ionized molecules of all other mass-to-charge ratios will not reach the collector. The ion current, the number of ionized molecules impinging on the collector per second, for this particular mass-to-charge ratio is displayed on a meter. The potentials applied to the rod are varied automatically and uniformly by a sweep generator, resulting in an oscilloscope display of the ion currents for all molecules in the mass-to-charge range of 1 to 50. The oscilloscope display can be recorded on a strip chart recorder. A typical gas spectrum is shown in Figure 4.

A residual gas analyzer displays a single gaseous compound as a series of peaks, known as a cracking pattern. The pattern includes the primary peak and a number of secondary peaks. The primary peak is due to the single ionization of the compound's molecules and occurs at a mass-to-charge ratio position corresponding to the molecular weight of the compound. Secondary peaks are due to isotopes, multi-

ple ionization of the molecules, and fragmentation of the molecules by the ionizing electrons. Each gaseous compound produces its own individual, repeatable cracking pattern. Cracking patterns are used to positively identify the individual components of a mixture of gases. Once the components are identified, their partial pressures may be determined if their analyzer sensitivities are known. The sensitivity of a gas is defined as the ratio of the ion current of the primary peak of the gas to the pressure of the gas in the analyzer section and is given in units of amps/Pa.

Interface System

The Veeco gas analyzer was connected to the shock tube by means of an interface system, shown in Figure 5, which was designed and constructed as part of this research. The Nupro needle valve and the Ultek 20 liter/sec ion pump were installed to maintain a sufficiently low pressure in the Veeco analyzer during analysis of the shock tube gas. A flexible coupling was included to facilitate attachment of the system to the shock tube. A pyrex section was added to electrically isolate the analyzer from the shock tube. To prevent charged particles from streaming into the analyzer when the shock tube was pulsed, a butterfly valve was installed. An ionization gauge tube was included to monitor the pressure in the analyzer section. In addition, an

up-to-air valve and an ion pump isolation valve were installed.

B. Sample Preparation and Surface Characterization

ATJ-S graphite samples were prepared from a 7.6 cm x 2.5 cm x 2.5 cm block of ATJ-S graphite, courtesy of Oak Ridge National Laboratories. Samples of cylindrical geometry with a diameter of 6 mm and a thickness of 15 mm were machined from the block. The wall thickness of graphite fusion reactor components is expected to be of this order.[11,28] One end was drilled and tapped to screw onto a sample holder rod. The other end, which was exposed to the plasma, was metallographically polished to near mirror (Linde B) smoothness. The entire specimen was then cleaned in distilled water in an ultrasonic cleaner and dried in an oven at 100°C for one hour.

Several samples of graphite were randomly selected after surface preparation and prepared for examination under a scanning electron microscope (SEM). The sample surfaces were examined and micrographs were taken of typical areas at magnifications ranging from 50 to 5,000 magnification. Micrographs of typical pre-exposed surfaces are shown in Figure 6.

C. Test Procedure

This investigation involved the irradiation of ATJ-S graphite in the shock tube and an analysis of the shock tube gas to identify hydrocarbon erosion products and to determine the impurity production rate.

Prior to these experiments, considerable work was performed on the shock tube and vacuum system to reduce background impurity levels to a minimum in order to facilitate residual gas analysis interpretation. It was necessary to thoroughly clean the walls of the shock tube and vacuum system to remove all hydrocarbon build-up resulting from prolonged use of an oil diffusion pump. This required the complete disassembly of the shock tube and vacuum system. All inner surfaces were cleaned with abrasives, dilute nitric acid, freon, and finally trichloroethylene. Trichloroethylene was used as a final cleaner because the peaks of its cracking pattern would not interfere with the present residual gas investigation. All O-ring surfaces and grooves were remachined and polished at this time to ensure good vacuum seals with new viton O-rings and teflon gaskets. A Sargeant-Welch model 3134 turbomolecular pump with 1500 ℓ/sec capacity was used instead of an oil diffusion pump to reduce oil backstreaming and subsequent recontamination of the inner surfaces of the shock tube and vacuum system.

After reassembly of the shock tube and vacuum system

and installation of the turbomolecular pump, the entire system was helium leak tested. The system was made as leak-tight as possible and attained a base pressure of 6.7×10^{-5} Pa. At this point, the residual gas analyzing system was coupled to the shock tube. Prior to experimentation, the shock tube was pulsed thirty times to discharge clean the inner surfaces. Cleaning ended when the post pulse gas pressure showed no increase for several consecutive pulses.

Six graphite samples were inserted into the shock tube and irradiated for 200 pulses at the incident ion energy of 800 ± 150 eV. Pulses were spaced a minimum of four minutes apart to allow sufficient pump down time between pulses. Gas analysis was performed after every fifth or tenth pulse and the residual gas spectrum was recorded. A residual gas spectrum of the background gases was also recorded at this time. Typical spectra are shown in Figure 7. After gas analysis following the 200^{th} pulse, the graphite samples were removed and replaced with six samples of PE-16, a high nickel stainless steel which had previously been studied in the shock tube by other investigators.[30,37,38] These samples were irradiated for 50 pulses at an incident ion energy of 800 ± 150 eV and gas analysis was performed after every tenth pulse. Typical spectra are shown in Figure 8. The purpose of this analysis was to determine which of the observed changes in the residual gas spectra

for graphite were due solely to the irradiation of graphite and which were merely due to pulsing the shock tube. After gas analysis following the 50^{th} pulse, the samples were removed.

Six additional graphite samples were irradiated for 40 pulses at an incident ion energy of 800 $\pm$ 150 eV and removed. These graphite specimens and those previously irradiated for 200 pulses at an incident ion energy of 800 eV were then examined under a scanning microscope and typical areas were photographed. No gas analysis was performed at this time.

A set of graphite samples were also irradiated at a lower incident energy of 250 $\pm$ 50 eV for 5, 25, 44, 50, 100, 150, and 200 pulses and removed. These specimens were examined under a scanning electron microscope and typical areas were photographed. No gas analysis was performed on this set.

D. Residual Gas Analyzer Calibration

The cracking patterns of several gases were determined to assist interpretation of the residual gas spectra. These gases included CH_4, N_2, H_2O, CO, HC_2Cl_3 (Trichloroethylene), and Ar. In addition, the analyzer sensitivities of several of these gases were determined. These results are found in section A of the results section.

IV. EXPERIMENTAL RESULTS

A. Cracking Pattern and Sensitivity Results

The cracking patterns and sensitivities were determined for several gases as mentioned earlier. These gases include CH_4, N_2, CO, H_2O, HC_2Cl_3 (Trichloroethylene), and Ar. The cracking patterns and sensitivities for these gases are found in Table 3.

Secondary peaks arise in the cracking patterns for H_2O, CH_4, and trichloroethylene from broken hydrogen bonds. The secondary peaks in the N_2, Ar, and CO cracking patterns arise from dissociation and double ionization.

B. Gas Analysis Results

Residual gas spectra were obtained after irradiation of the graphite and stainless steel samples, as noted in the previous section, to identify hydrocarbon erosion products and to determine the impurity production rate. Before analyzing this data, it was necessary to perform two more tasks. First, it was necessary to determine which deuterated hydrocarbons were most likely to form from the erosion of graphite and to determine the peaks associated with each product. Second, it was also necessary to determine which other gases and impurities were present in the vacuum system and to determine whether these produced peaks, as de-

termined from cracking pattern results, which would overlap those of the hydrocarbon erosion products.

With regard to the first point, from a review of previous literature[11-29], CD_4 (CH_4) and C_2D_2 (C_2H_2) have been the only hydrocarbon erosion products observed. Since in this investigation, graphite was bombarded by deuterium ions, the erosion products expected were CD_4 and C_2D_2. The peaks associated with CD_4 occur at the mass-to-charge ratios of 12, 14, 16, 18, and 20 while the peaks associated with C_2D_2 occur at 24, 26, and 28.

With regard to the second point, the background gases and impurities present in the vacuum system can easily be determined by simple considerations. Since the base pressure of the shock tube is only 6.7×10^{-5} Pa and the pumping section was closed off during firing, atmospheric constituents such as N_2, O_2, H_2, CO_2, and Ar should be expected with peaks at 14 and 28; 16 and 32; 1 and 2; 12, 14, 16, 28, 29, and 30; and 20 and 40, respectively. Since the system was unbaked, large quantities of H_2O should be present with peaks at 16, 17, and 18. Remnants of trichloroethylene, a solvent used to clean the inner surfaces of the shock tube and vacuum system, should be seen at 35, 36, 37, and 38. In addition, organic impurities such as CH_4, $CH_3CH_2^+$, and CH_2CH^+ should be seen at low levels. These impurities occur in all vacuum systems utilizing oils or bearing lubricants.[39]

Several additional peaks should occur as a result of the substitution of deuterium for hydrogen atoms. Contributions to each observed peak in the mass-to-charge ratio range of 1 to 50 are listed in Table 4 on the basis of this analysis.

The residual gas spectra obtained for graphite and stainless steel were initially analyzed for the presence of CD_4. This was done by taking the 20 peak, the primary peak for CD_4, and subtracting the contribution from argon as determined from the observed height of the primary argon peak at 40 and cracking pattern data. Then the background was deducted, as determined by the background gas spectrum, to give the amount of CD_4 produced only as a result of the one shock tube pulse prior to gas analysis. This data is produced in Figure 9 for both graphite and stainless steel spectra. Notice that there remains a contribution to the 20 peak for graphite but none for stainless steel indicating that the contribution is a result of the erosion of graphite. To positively identify this product as CD_4, the 16 and 18 peaks were also analyzed in the case of graphite and the results were compared to the cracking pattern for CD_4. After subtraction of the contributions from other gases and correction for background, the remaining contributions were plotted and are shown in Figure 10. A comparison of the experimental results with cracking pattern results is seen in Table 5. The agreement is seen to be very good. It is

therefore concluded that CD_4 is a product of the erosion of graphite, in agreement with the results of previous investigators.[11-29]

Notice that the amount of CD_4 produced after each pulse, as determined by the height of the 16, 18, and 20 peaks, is relatively constant after each pulse during the course of the 200 pulse experiment. This indicates that surface conditioning did not occur to any significant degree during this investigation.

The observed spectra were also analyzed for the presence of C_2D_2. The 28 peak could not easily be used to determine the presence of C_2D_2 because of the large contribution to this peak from N_2 arising from the erosion of the boron nitride reflecting wall. Instead, the 24 and 26 peaks were examined. However, after correction for other gases and background, results showed that there were no differences between results for graphite and stainless steel indicating that C_2D_2 is not a significant erosion product of graphite under the present experimental conditions. There existed no evidence of any other hydrocarbon erosion product. These results agree with previous results which found no other erosion product for bombardment by energetic ions.[11,17-29]

C. Impurity Production Rate

Since the gas analyzer sensitivity for CD_4 was pre-

viously determined, the partial pressure of CD_4 in the analyzing section was calculated and was found to be 9.3×10^{-6} Pa for an average peak height of 0.92×10^{-12} amps for the 20 peak. This corresponds to a partial pressure of CD_4 in the shock tube of 2.1×10^{-1} Pa after making the necessary corrections for flow through a needle valve. Applying the ideal gas law, the partial pressure of CD_4 can be converted into the number of molecules of CD_4 produced for each pulse of the shock tube. Since the number of energetic deuterium ions striking the graphite samples per shock tube pulse is known, $1 \pm .25 \times 10^{16}$ ions/cm^2, the impurity production rate can be determined. The impurity production rate for hydrocarbons was found to be 18 ± 12 carbon atoms per incident deuterium ion. This value of impurity production rate cannot be explained by such classical erosion mechanisms such as physical and chemical sputtering where the impurity production rate cannot exceed unity. It indicates, instead, that the erosion of graphite by a hot, dense deuterium plasma is mainly due to other erosion mechanisms such as arcing or sublimation. For these erosion mechanisms, an impurity production rate can exceed unity.

D. Surface Analysis Results

As mentioned, sets of graphite samples were exposed in the shock tube to a deuterium plasma at mean incident ion

energies of 250 eV and 800 eV. Surface examination was performed in a scanning electron microscope at 35 to 5000 magnification for the 250 eV samples exposed for 5, 25, 44, 50, 100, 150, and 200 pulses and for the 800 eV samples exposed for 40 and 200 pulses. Typical surface areas of these samples are shown in Figures 11-17. Micrographs of the surfaces of unexposed samples are included for comparison.

Three distinct areas can be identified on all exposed and unexposed specimen surfaces. The first area is the area at the pore edges and appears almost white in the micrographs. This is due to electron saturation in the scanning electron microscope at these areas. Erosion at the pore edges from deuterium bombardment is seen to increase as the radiation dose increases. The sharp edges eventually become smooth and rounded.

The second area is an area which appears very dark gray or black in the micrographs. This dark area represents solid, bulk graphite and is dark because of the good conduction of scanning electron microscope electrons from the surface region. The areas appear smooth with extremely fine surface features. Erosion of these fine features in the dark areas increases with dosage.

The third area appears light gray in the micrographs. These areas represent pores hidden below the surface. They appear lighter in shade than the bulk areas because conduc-

tion of scanning electron microscope electrons from the thin surface layer is reduced, resulting in a slight overcharging of the layers. On the exposed samples, the thin surface layers appear flaked, buckled, and displaced and exhibit a large amount of surface area. Micrographs show the erosion of these thin layers at various stages. The coverage of the surface by these light gray areas increases with exposure at the expense of the darker regions indicating that there is an enhancement of erosion at the sub-surface pore regions. Successive enlargements of a sub-surface pore region is seen in Figure 16.

A comparison of micrographs of graphite specimens exposed to the same number of pulses but to different mean incident ion energies shows that a significantly greater amount of erosion occurs at 800 eV than at 250 eV. This is seen in Figure 17.

V. DISCUSSION AND ANALYSIS

This experimental investigation has been successful with respect to achieving its original goals:

1) Methane (CD_4) has been identified as the sole hydrocarbon erosion product of ATJ-S graphite under the existing experimental conditions.

2) The impurity production rate for ATJ-S graphite has been determined and is found to be 18 ± 12 carbon atoms per incident deuterium ion for bombardment by a deuterium plasma with an incident ion flux of $1 \pm .15 \times 10^{23}$ ions/cm^2-sec and a mean ion energy of 800 ± 150 eV.

3) Distinct features and trends in the erosion of the ATJ-S graphite surface have been identified.

These results will be discussed further in this section. It will also be shown in this section that:

1) The major impurity production mechanism, or erosion mechanism, is not chemical or physical sputtering, but is probably arcing or sublimation.

2) The surface flaking is due to the thermal expansion of the graphite grains.

A. Validity of the Present Investigation

Residual gas analysis is usually performed in an ultra-high vacuum system in which all background gases and im-

purities are minimal. In such a system, gas analysis is straightforward and unambiguous and the results are unequivocal. Unfortunately, the design and operation criteria for an ultra-high vacuum system are incompatible with the design and operation criteria for a shock tube. As a result, the lowest base pressures attainable in the shock tube are in the low 10^{-5} Pa range. At these pressures, background gases and impurities can complicate analysis.

However, in this study, the significant differences in observed gas spectra for graphite and PE-16 stainless steel certainly eliminates any doubt as to the presence of CD_4 as an erosion product of graphite. The actual amount of CD_4 produced per pulse, though is less certain. The contributions of other molecular species to the CD_4 gas peaks and the accumulation of gases during the course of the experiment introduce some amount of error into the determination of the impurity rate. The experimental error from these uncertainties is estimated to be $\sim$30%. The total experimental error is estimated, quite liberally, to be no more than $\sim$75%.

It should be pointed out that the use of the vacuum system presently employed on the shock tube does have an advantage in that it is almost identical to the type of vacuum systems presently being employed on experimental tokamaks and envisioned for use on future tokamaks. Hence, the vac-

uum environment found in the shock tube, with its background gases and impurities, is similar to the vacuum environment found in present day tokamaks and expected to exist in future tokamaks.

B. Surface Erosion and Flaking

The results of this experiment indicate that considerable erosion of the graphite surface occurs under energetic ion bombardment at high incident fluxes of $\sim 10^{23}$ ions/cm^2-sec. The principal erosion areas are those areas lying directly above sub-surface pores in which the layer of graphite is quite thin — $\sim$1 μm or less in thickness. These layers also appear flaked and fractured. The pore edges also exhibit considerable erosion while the flat, bulk surface exhibits only mild erosion. However, no flaking or cracking occurs in these two regions.

The heat flux to the sample surface can be calculated to see if the heat flux is responsible for the observed surface flaking and cracking. If all the incident ions deposit all their energy during the 0.1 μsec of interaction for each pulse, then the heat flux is 15 x 10^6 watts/m^2 and 48 x 10^6 watts/m^2 for bombardment by 250 eV and 800 eV particles, respectively.

The maximum heat flux, W_{CR}, which can be sustained by a material of thickness, ℓ, whose back surface is cooled,

without exceeding the material yield stress is given by[40]:

$$W_{CR} = \frac{C^{*}\pi^{2}K(1-v)\sigma_{max}}{\ell E \alpha} \qquad (1)$$

where v is Poisson's Ratio, σ_{max}, is the ultimate compressive strength, ℓ is the material thickness, E is Young's Modulus, α is the coefficient of thermal expansion, C^{*} is a constant with a value of order 8 and K is a constant between 0.5 and 2.5 which depends on geometry. For typical values[41] of K, v, σ_{max}, E, and α for ATJ-S graphite we obtain the following expression:

$$W_{CR} = \frac{1.8 \times 10^{5}}{\ell} \frac{\text{watts}}{m^{2}} \qquad (2)$$

when ℓ is given in meters. For ATJ-S graphite, the maximum value of ℓ, which yields the minimum value of W_{CR}, is the average grain size which is ~ 200 μm. Hence, we have

$$W_{CR} \gtrsim 9.0 \times 10^{8} \text{ watts/m}^{2} \qquad (3)$$

which is significantly greater than the maximum imposed experimental heat flux of $\sim 48 \times 10^{6}$ watts/m^{2}.

According to this, then, cracking and flaking should not occur anywhere on the graphite surface. This conclusion

is supported, in the bulk areas, but not in the thin regions above sub-surface pores. This implies that a different type of cracking mechanism is in effect, which can occur at lower heat fluxes. An examination of the cracking, as seen in Figure 16, shows that cracking occurs primarily where the thin layer joins the bulk region. This seems to imply that the lateral stress arising from thermal expansion of the bulk cannot be supported across the thin layer. The situation is shown schematically in Figure 17 in a simplified version where the graphite bulk and thin regions are shown as separate entities.

To calculate the stress on the thin region, it is necessary to determine the temperature of the surface. Knowing the heat flux to the sample surface, the surface temperature rise can be computed using[42]

$$T = 2W\sqrt{\frac{t}{KCp}} \qquad (4)$$

where W is the heat flux, t is the time of application of the heat flux, K is the thermal conductively, C is the specific heat, and p is the material density. For typical values[41] of K, C, and p, and for an interaction time of 0.1 μsec, we have

$$T = W \times 6 \times 10^{-8}\ ^{o}K \qquad (5)$$

when W is given in watts/m^2. For values of W as previously determined, we find that the temperature at the surface of the bulk regions rises to $\sim 900^{o}C$ and $\sim 2{,}880^{o}C$ for irradiation by 250 eV and 800 eV particles, respectively. Using the lower value of temperature and the coefficient of thermal expansion, the change in length of a 200 μm grain is ~ 0.26 μm which implies that the strain on a thin region of length 5 μm, surrounded on two sides by large grains, is $\sim 5\%$. This results in a compressive stress of $\sim 4.5 \times 10^{8}$ nt/m^2, which is far in excess of the maximum compressive stress[41] of $\sim 5.5 \times 10^{7}$ nt/m^2. Therefore, it seems that the flaking of the thin regions is due to thermal stresses arising in the bulk grains which cannot be supported across the thin layered region.

C. Erosion and Impurity Production Mechanisms

In addition to flaking and cracking, the thin regions appear to suffer considerably more erosion than the bulk regions. A proposed erosion mechanism for graphite must be consistent with this observation and the experimentally determined impurity production rate.

The impurity production rate determined in this investigation- $1.8 \pm 1.2 \times 10^{1}$ molecules/ion -is considerably

greater than unity. This suggests that erosion mechanisms such as physical and chemical sputtering do not play a major role in the erosion of the graphite surface since it is difficult to envision a mechanism whereby these processes could produce a impurity production rate in excess of unity. Other possible mechanisms are evaporation and sublimation. It has been shown that the maximum temperatures on the graphite surface are $\sim 900^{\circ}C$ and $\sim 2,880^{\circ}C$ for particle energies of 250 eV and 800 eV, which are considerably below the sublimation temperature of $3,350^{\circ}C$. At these temperatures, evaporation is minimal. However, these maximum temperatures are correct only for the bulk material, which indeed showed little erosion at all. It is possible that heat conduction is severly reduced in the thin regions, due to a reduction in the mean free path for conduction, resulting in temperatures approaching or exceeding the sublimation temperature. This would account for the enhanced erosion of the thin areas. However, it is impossible to determine the impurity production rate resulting from evaporation or sublimation since in this case they would not be a bulk phenomena.

Arcing is another possible erosion mechanism and impurity production mechanism. Since arcing involves a current loop between the plasma and the material surface, as originally suggested by Robson[43], which can produce intense, localized heating, resulting in melting and vaporization,

impurity production rates in excess of unity are possible. Evidence of arcing consists of arc craters or arc tracks on the sample surface which form as a result of surface melting and subsequent resolidification. These remnants of arcing are easily visible on surfaces polished to a mirror finish.

Arcing is known to occur in the shock tube.[30,37,38] All materials tested prior to graphite by previous investigators exhibited evidence of significant amounts of arcing in the form of arc craters. These other materials include: 304 stainless steel; 316 stainless steel; PE-16, a high nickel stainless steel; 4130 steel; Ti-6Al-4V; tungsten; niobium; and copper.

There is no direct evidence of arcing on the surfaces of the graphite samples exposed in the shock tube during this investigation. However, this is not at all suprising since graphite sublimes, rather than melts. Arcing damage could be considerably different from that observed on materials which can melt. Also, since graphite can not be polished to a mirror finish, evidence of arcing may be indistinguishable from other surface features. Hence, the lack of evidence for arcing does not preclude the possible occurrence of arcing. Arcing may have occurred but may not have left behind any recognizable surface remnants of arcing. The occurrence of observable arcing damage, in the form of long ridges, on the surface of graphite limiters exposed in

tokamaks may be due to arcing of higher intensity and of longer duration than that which occurs in the shock tube.

Arcing could produce the higher erosion observed on the thin layered regions. Previous studies on arcing have suggested that structural discontinuities and interfaces increase the potential for arcing.[44-47] Since the thin layered regions are characterized by flaked and fractured surfaces which contain innumerable discontinuities and interfaces, arcing erosion would be more severe in these regions than in bulk regions resulting in a higher degree of erosion in the thin layered regions.

The observed erosion product of graphite was CD_4, a product usually associated with chemical sputtering. However, chemical sputtering does not seem to be a likely erosion mechanism in this study. The proposed erosion mechanisms, sublimation and arcing, result in the release of carbon atoms from the graphite surface. Hence to account for the large presence of CD_4, it seems that the carbon atoms released from the surface by the proposed mechanisms of erosion must combine with deuterium ions in the plasma to produce CD_4.

D. Comparison of Results with Previous Work

The results of the present investigation are in agreement with the results obtained for graphite in experimental tokamaks[25-27] which showed that CD_4 levels increase appreciably

as a result of plasma bombardment and that arcing is a major erosion mechanism.

Comparison of the present results with results obtained using ion beams, shows that ion beam experiments do not accurately predict the impurity production rate for graphite under plasma bombardment. Ion beam results for the impurity production rate — 2.5×10^{-2} to 1.5×10^{-1} molecules/ion — are significantly lower than the results obtained in this experiment — 18 ± 12 molecules/ion. This significant difference is attributed to the absence of electrons in the ion beam experiments which precludes arcing as an erosion mechanism and to the low incident particle fluxes used in the ion beam experiments which preclude significant amounts of sublimation.

VI. CONCLUDING REMARKS

The present results show that flaking occurs only above sub-surface pores and is due to lateral stresses arising from the thermal expansion of the surface region. Erosion is also observed to occur predominantly above the sub-surface pore regions and may be related to the flaking process. This suggests that flaking, erosion, and the impurity production rate may be significantly reduced by using other types of graphite that contain no pores and have a low coefficient of thermal expansion in the surface plane, which would reduce the lateral stresses in the surface region. Further studies should be undertaken to evaluate the performance of these other types of graphite under plasma bombardment.

The need for a low expansion coefficient in the surface plane suggests the use of a graphite with a columnar grain structure in which the c-axes of the grains are all oriented perpendicular to the surface plane. This orientation places the a-axes of the grains in the surface plane and reduces the lateral stresses in the surface region since, in graphite, the thermal expansion coefficient is a minimum in the a-axis direction.

A graphite with a columnar grain structure and no pores can be utilized either in bulk form or as a graphite

coating on some substrate material. At present, however, the availability of a bulk graphite with an extremely low pore volume is questionable. Most bulk graphites have porosities in excess of 15%. The fabrication of a bulk graphite with low or zero porosity and a columnar structure may require considerable modification of the present fabrication techniques. Graphite coatings, however, appear to be quite attractive. With proper growth techniques, a thin graphite coating with a columnar grain structure and low pore volume should be attainable by present vapor deposition methods. These coatings need not be more than ten to twenty microns in thickness, judging by the amount of damage observed in this study on the bulk surfaces of ATJ-S graphite. However, these columnar grain structures in thin coatings typically have weak grain boundary adhesion perpendicular to the thermal shock direction which may cause serious cracking problems. In addition, the adhesion of the coating to the substrate may be a serious problem especially if metals are used as the substrate material. Metals typically have thermal expansion coefficients that are significantly larger than the thermal expansion coefficient of graphite.

This investigation has also shown that the number of methane molecules formed per incident ion during the plasma bombardment of ATJ-S graphite exceeds unity. This implies that the formation of impurity molecules is probably due to

such erosion processes as arcing, or sublimation, or some combination of both. However, the calculation for an impurity production rate usually assumes that the number of impurity atoms formed actually correlates with the incident ion flux. Is this a valid assumption to make in the present investigation?

For an impurity production mechanism such as sublimation, the correlation clearly exists. The incident ion flux determines the rise in surface temperature which determines the number of carbon atoms leaving the surface through sublimation. However, for arcing, the correlation is not clear. The number of impurity atoms produced through arcing may be more dependent upon the electrical conditions at the wall of the device during a discharge than on the incident ion flux. In fact, the electrical conditions at the wall is one area where shock tube simulation may be markedly different from a tokamak limiter.

If correlation does exist between the number of impurity molecules formed and the incident ion flux, as is the case for sublimation, the present results can be readily extended to a tokamak reactor. A calculation can then be made to estimate the carbon impurity concentration that one would expect to find in a tokamak reactor under steady-state conditions. This value can then be compared to the critical impurity concentration for carbon atoms to evaluate graphite

as a fusion reactor material. These calculations can be found in the Appendix. The results of the analysis show that impurity production can be a serious, but not a critical, problem for ATJ-S graphite.

In conclusion, this investigation has shown that ATJ-S graphite does not experience serious surface damage and hence, maintains its structural integrity under bombardment by a hot, dense deuterium plasma. In addition, it has been shown that the influx of impurities into the plasma may occur primarily through such erosion mechanisms as unipolar arcing and sublimation rather than through chemical or physical sputtering. If this is the case in a tokamak reactor, the introduction of impurities must be carefully evaluated for a real tokamak.

PAGES 41 to 42

WERE INTENTIONALLY

LEFT BLANK

REFERENCES

1. R. Behrisch, J. Nucl. Mat., 85 & 86, 1047, (1979)

2. W. Bauer, J. Nucl. Mat., 76 & 77, 3, (1978)

3. G.M. McCracken and P.E. Stott, Nuclear Fusion, 19, 889, (1979)

4. B.M.U. Scherzer, R. Behrisch, and J. Roth, Proc. Int. Symp. Plasma-Wall Interactions (Julich 1976), Pergamon Press, Oxford, (1977), p. 353

5. D.M. Meade, Nuclear Fusion, 14, 289, (1974)

6. R.V. Jensen, D.E. Post, W.H. Grasberger, C.B. Tarter, and W.A. Lokke, Nuclear Fusion, 17, 1187, (1977)

7. R.V. Jensen, D.E. Post, and D.L. Jassby, Plasma Physics Laboratory Princeton, Rep. PPPL-1350, (1977)

8. R.W. Conn and J. Kesner, J. Nucl. Mat., 63, 1, (1976)

9. M.J. Davis, Tokamak Materials Workshop, Sandia Laboratory, Albuquerque, N.M., 18-19, July 1977

10. R.G. Mills, ed., "A Fusion Power Plant", MAT7-1050, Princeton Plasma Physics Lab., Princeton, N.J., (1974)

11. R.A. Langley, R.J. Colchin, R.C. Isler, M. Murakami, J.E. Simpkins, J. Cecchi, V.L. Corso, H.F. Dylla, R.A. Ellis, Jr., and M. Nishi, J. Nucl. Mat., 85 & 86, 215, (1979)

12. B.J. Wood and H. Wise, J. Phys. Chem., 73, 1348, (1969)

13. R.K. Gould, J. Chem. Phys., 63, 1825, (1975)

14. M. Balooch and D.R. Olander, J. Chem. Phys., 63, 4772, (1975)

15. G.M. McCracken and J.W. Partridge, J. Nucl. Mat., 63, 373, (1976)

16. S. Veprek, M.R. Haque, and H.R. Oswald, J. Nucl. Mat., 63, 405, (1976)

17. B. Feinberg and R.S. Post, J. Vac. Sci. Tech., 13, 443, (1976)

18. R. Behrisch, J. Bohdansky, G.H. Oetjen, J. Roth, G. Schilling, and H. Verbeek, J. Nucl. Mat., 60, 321, (1976)

19. J. Roth, J. Bohdansky, W. Poschenrieder, and M.K. Sinha, J. Nucl. Mat., 63, 222, (1976)

20. N.P. Busharov, E.A. Gorbatov, V.M. Gusev, M.I. Guseva, and Yu.V. Martynenko, J. Nucl. Mat., 63, 230, (1976)

21. S.K. Erents, C.M. Braganza, and G.M. McCracken, J. Nucl. Mat., 63, 399, (1976)

22. K. Sone, H. Ohtsuka, T. Abe, R. Yamada, K. Obara, O. Tsukakoshi, T. Narusawa, T. Satake, M. Mizuno, S. Komiya, Proc. Int. Symp. Plasma-Wall Interactions (Julich 1976), Pergamon Press, Oxford, (1977), p. 323

23. J.N. Smith, Jr., C.H. Meyer, Jr., and J.K. Layton, J. Nucl. Mat., 67, 234, (1977)

24. C. Braganza, S.K. Erents, and G.M. McCracken, J. Nucl. Mat., 75, 220, (1978)

25. J. Bohdansky, H.L. Bay, and W. Ottenberger, J. Nucl. Mat., 76 & 77, 163, (1978)

26. J.A. Borders, R.A. Langley, and K.L. Wilson, J. Nucl. Mat., 76 & 77, 168, (1978)

27. J.N. Smith, Jr. and C.H. Meyer, Jr., J. Nucl. Mat., 76 & 77, 193, (1978)

28. R.J. Colchin, C.E. Bush, P.H. Edmonds, A.C. England, K.W. Hill, R.C. Isler, T.C. Jernigan, P.W. King, R.A. Langley, D.H. McNeill, M. Murakami, R.V. Neidigh, C.H. Neilson, J.E. Simpkins, J. Wilgen, J.C. DeBoo, K.H. Burrell, and E.S. Ensberg, J. Nucl. Mat., 76 & 77, 405, (1978)

29. T. Hirayama, N. Fujisawa, Y. Gomay, M. Maeno, K. Uehara, M. Shimada, N. Suzuki, T. Yamamoto, S. Konoshima, J. Nucl. Mat., 76 & 77, 452, (1978)

30. N.F. Panayotou, Doctoral Thesis, Columbia University, New York, N.Y., also Columbia University Plasma Lab Report No. 78, (1978)

31. R.A. Gross, Reviews of Modern Physics, 37, 724, (1965)

32. B. Feinberg, J. Plasma Physics, 18, 265, (1976)

33. B. Jensen, Phys. of Fluids, 20, 373, (1977)

34. L. Scaturro and T.C. Marshall, Phys. of Fluids, 20, 38, (1977)

35. D. McNeill, Phys. of Fluids, 18, 44, (1975)

36. S. Robertson and Y.G. Chen, Phys. of Fluids, 18, 917, (1975)

37. N.F. Panayotou, J.K. Tien, and R.A. Gross, J. Nucl. Mat., 63, 137, (1976)

38. J.K. Tien, N.F. Panayotou, R.D. Stevenson, and R.A. Gross, J. Nucl. Mat., 76 & 77, 481, (1978)

39. L. Maurice, P. Duval, and G. Garinas, J. Vac. Sci. Tech., 16, 741, (1979)

40. J.F. Schivell and D.J. Grove, J. Nucl. Mat., 53, 107, (1974)

41. C.L. Mantell, "Carbon and Graphite Handbook", Interscience Publishers, N.Y., (1968)

42. H.S. Carslaw and J.C. Jaeger, "Conduction of Heat in Solids", 2nd ed., Oxford University Press, Oxford, p. 401, (1959)

43. A.E. Robson and P.C. Thonemann, Proc. Phys. Soc., 73, 508, (1959)

44. R.P. Little and W.T. Whitney, J. Appl. Phys., 34, 2430, (1963)

45. T.J. Fibiniak, L. Jedynak, and R.A. Dodd, J. Appl. Phys., 42, 2240, (1971)

46. E. Hantzskhe, B. Juttner, V.F. Puchkarov, W. Rohrbeck, and H. Woltt, J. Phys. D., 9, 1771, (1976)

47. J.D. Cobine, "Gaseous Conductors", Dover Publications Inc., N.Y., (1958)

Figure 1. A plot of the minimum value of the product of the plasma number density and plasma energy confinement time, nt, for ignition of a deuterium-tritium plasma vs. the impurity fraction for several impurities at plasma temperatures of 10 keV and 20 keV. (Taken from R.V. Jensen et.al., Nuclear Fusion, 17, 1187, 1977)

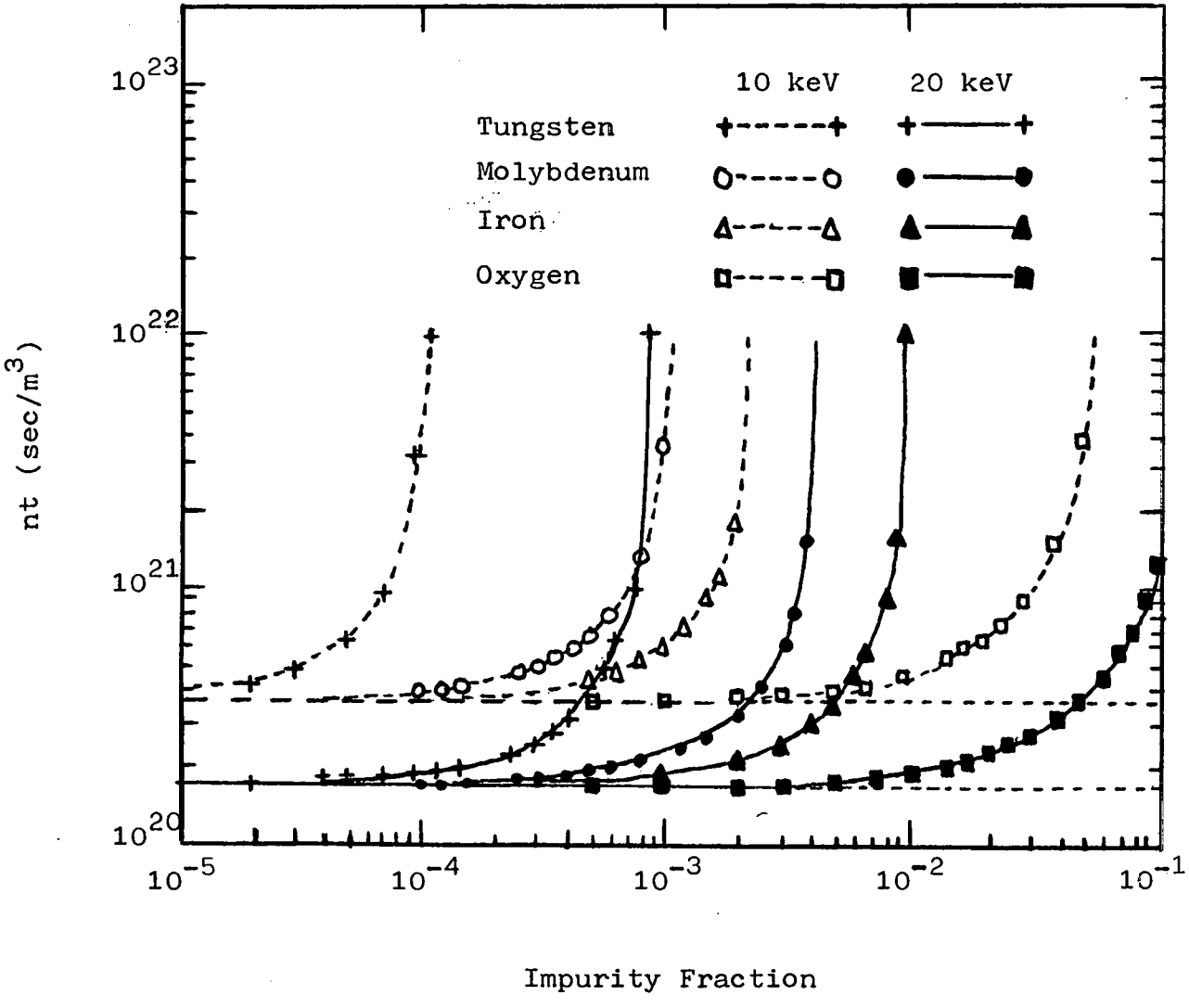
10 keV
20 keV
Tungsten
Molybdenum
Iron
Oxygen
10^{23}
10^{22}
10^{21}
10^{20}
nt (sec/m^3)
10^{-5}
10^{-4}
10^{-3}
10^{-2}
10^{-1}
Impurity Fraction

Figure 1

Figure 2. A plot of the maximum allowed impurity concentration for fusion for several impurities vs. plasma temperature. (Taken from R.V. Jensen et.al., Plasma Physics Laboratory Princeton, REP. PPPL-1350, 1977)

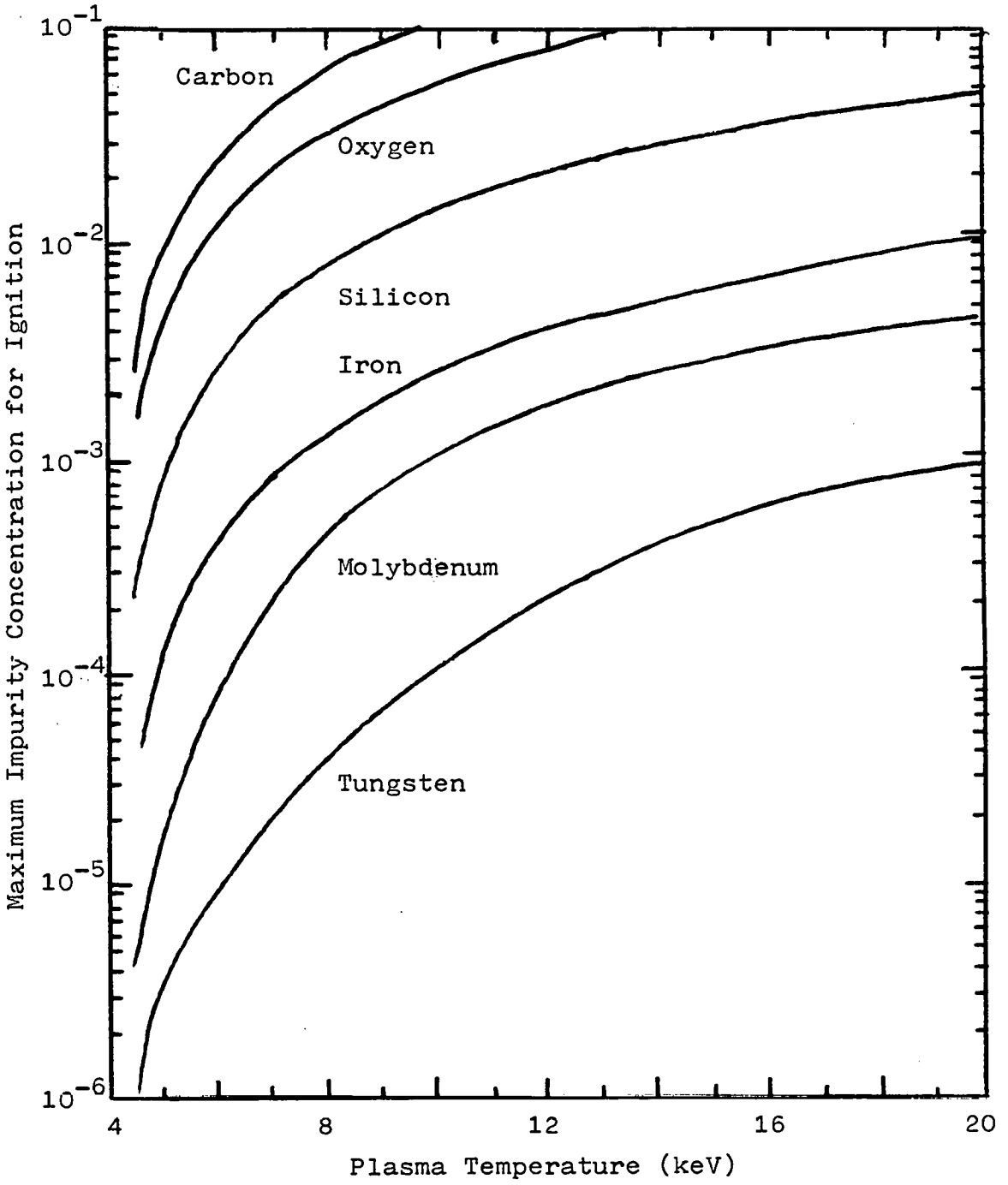
Maximum Impurity Concentration for Ignition
10^{-1}
10^{-2}
10^{-3}
10^{-4}
10^{-5}
10^{-6}
Carbon
Oxygen
Silicon
Iron
Molybdenum
Tungsten
4
8
12
16
20
Plasma Temperature (keV)

Figure 2

Figure 3. A schematic of the Columbia University Electromagnetic Shock Tube.

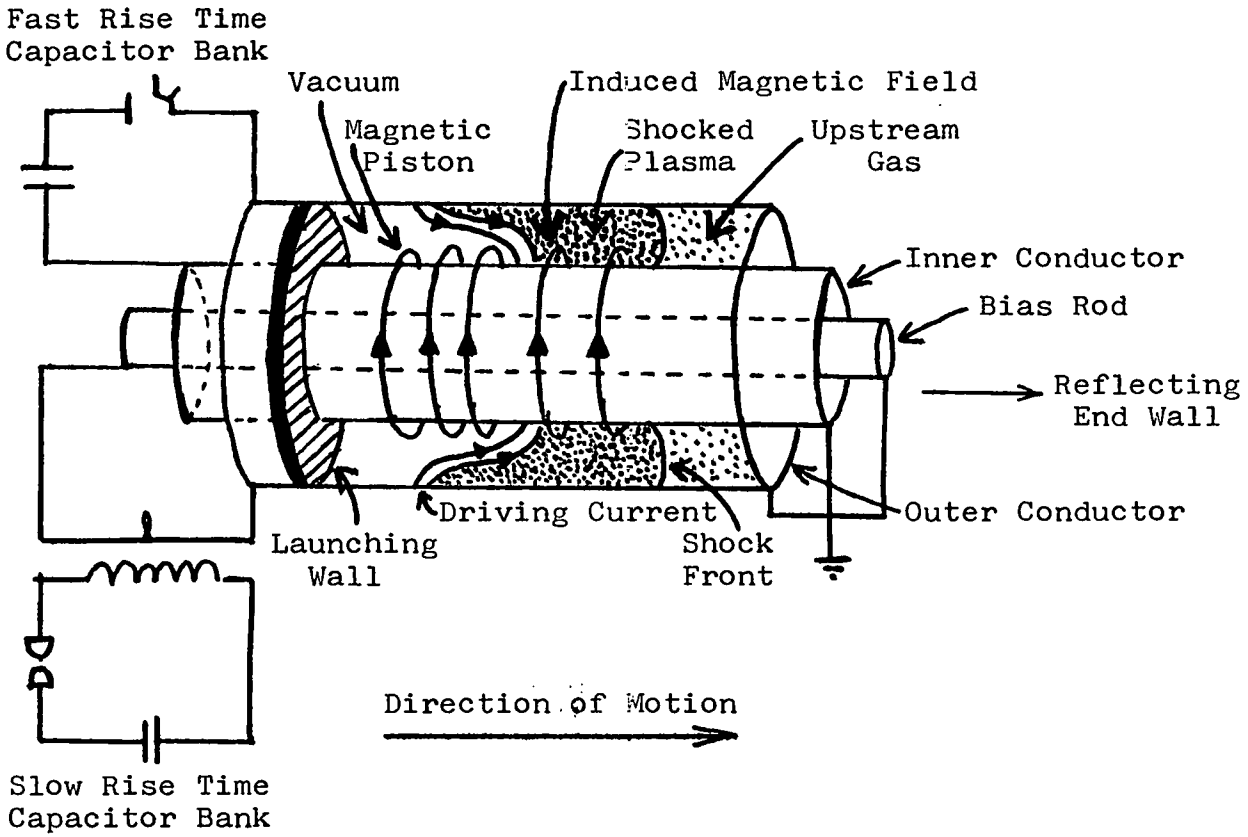
Fast Rise Time
Capacitor Bank
Vacuum
Induced Magnetic Field
Magnetic
Piston
Shocked
Plasma
Upstream
Gas
Inner Conductor
Bias Rod
Reflecting
End Wall
Outer Conductor
Driving Current
Launching
Wall
Shock
Front
Direction of Motion
Slow Rise Time
Capacitor Bank

Figure 3

Figure 4. A typical residual gas analyzer spectrum. This spectrum was recorded after plasma bombardment of ATJ-S graphite for 60 shock tube pulses.

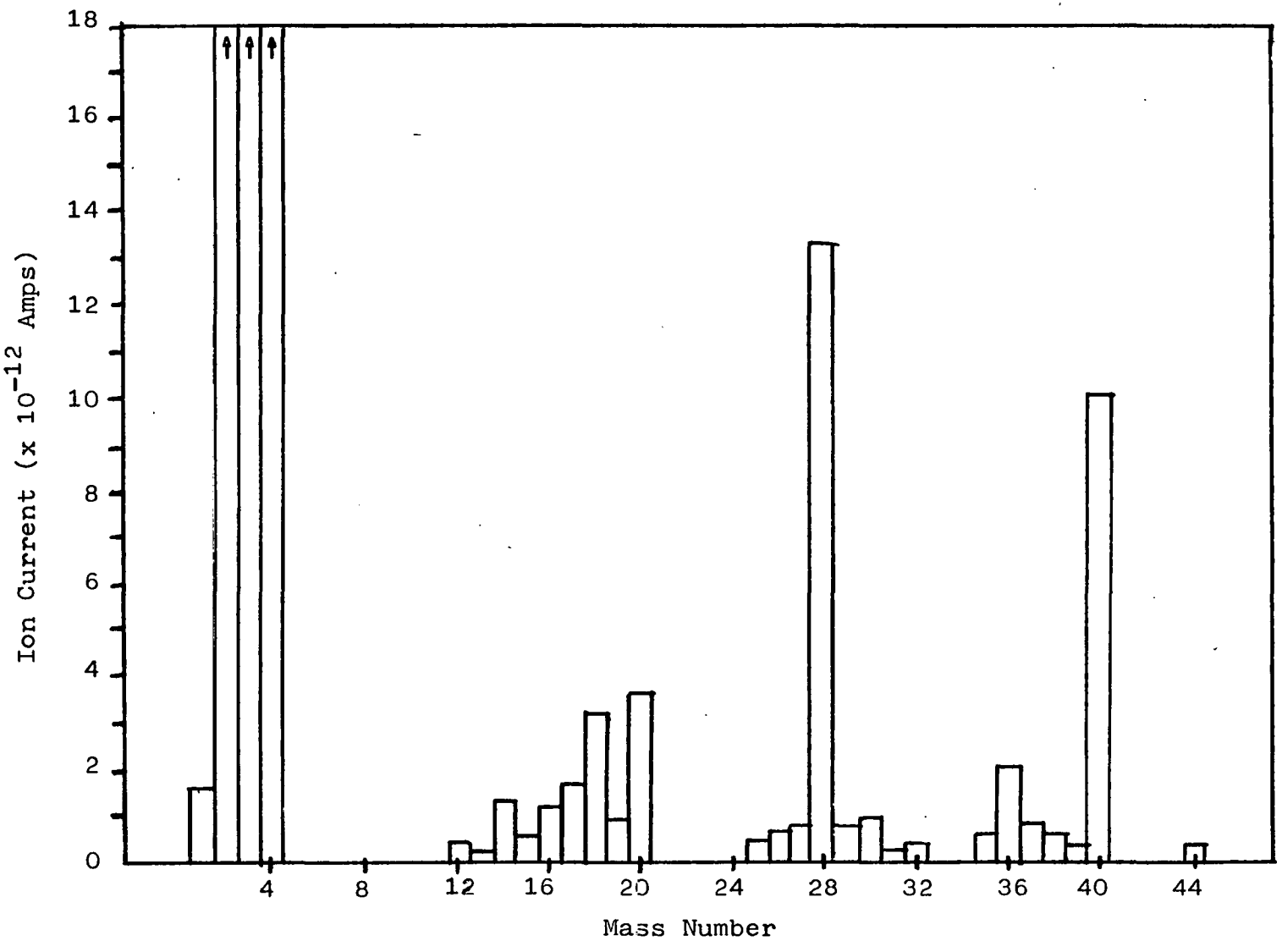
Ion Current (x 10^{-12} Amps)
0
2
4
6
8
10
12
14
16
18
4
8
12
16
20
24
28
32
36
40
44
Mass Number

Figure 4

Figure 5. A schematic of the interface system that coupled the residual gas analyzer to the shock tube.

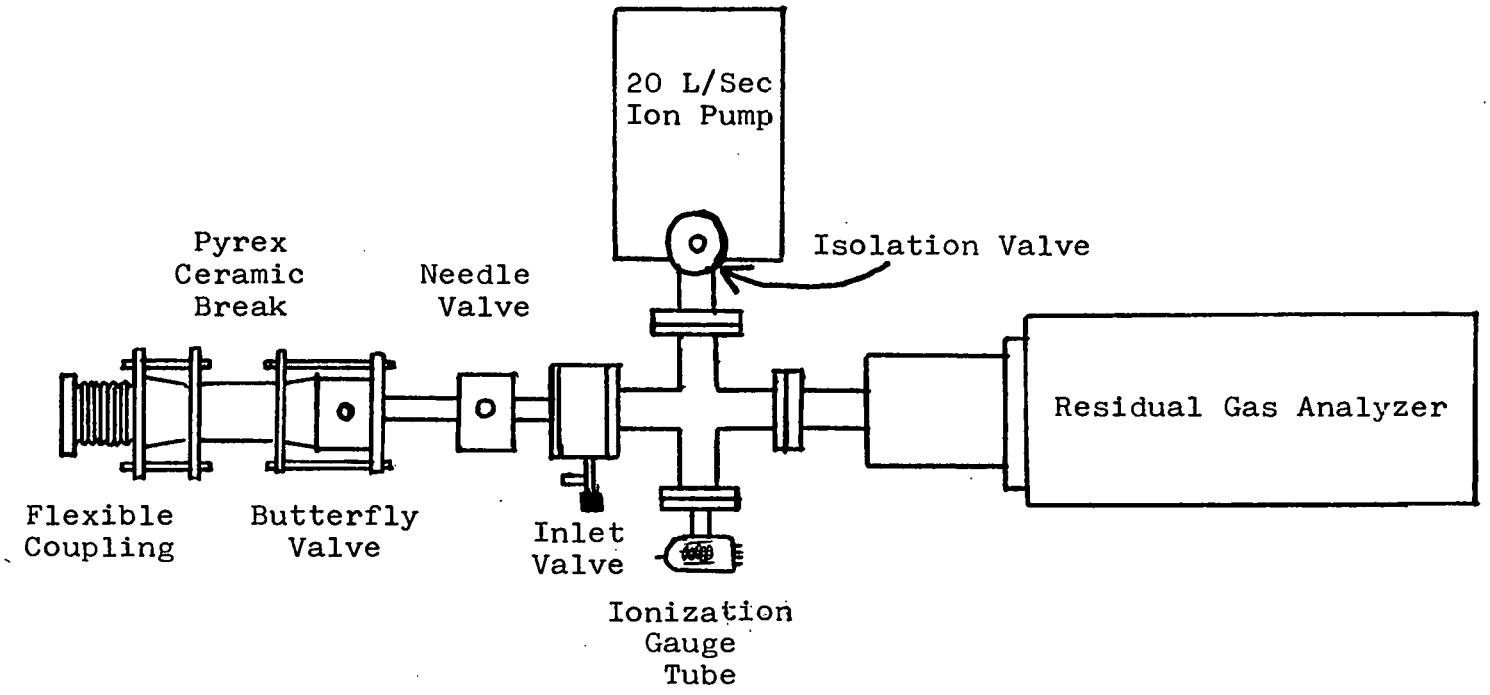
20 L/Sec
Ion Pump
Isolation Valve
Pyrex
Ceramic
Break
Needle
Valve
Residual Gas Analyzer
Flexible
Coupling
Butterfly
Valve
Inlet
Valve
Ionization
Gauge
Tube

Figure 5

Figure 6. SEM micrographs of typical areas of the unexposed, polished surface of ATJ-S graphite.

(A)

(B)

(C)

(D)

FIGURE 6

Figure 7. Typical post-pulse (A) and background (B) residual gas spectra for ATJ-S graphite. These spectra were recorded after exposure of ATJ-S graphite samples to 60 shock tube pulses.

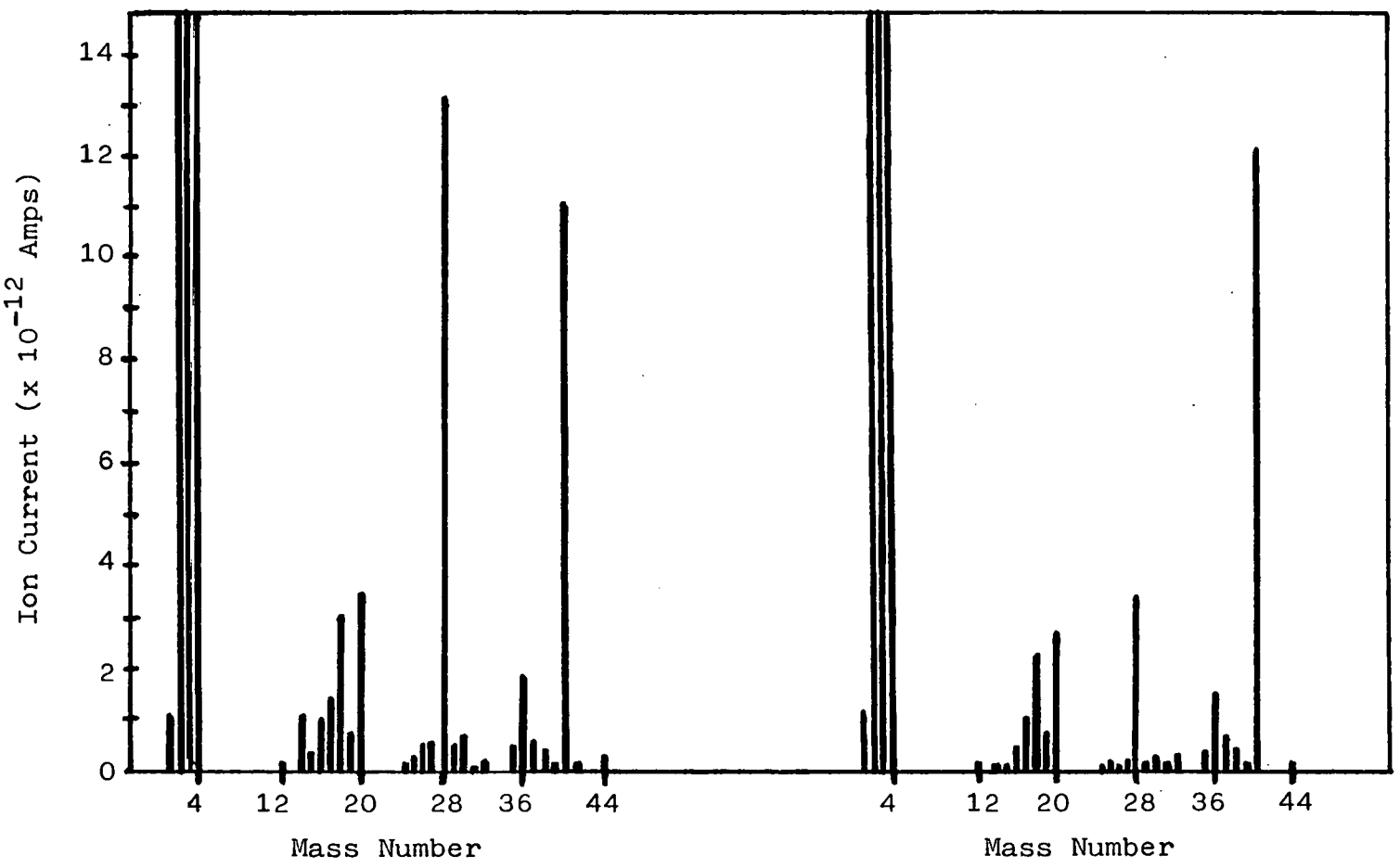
Ion Current (x 10^{-12} Amps)
0
2
4
6
8
10
12
14
4
12
20
28
36
44
Mass Number
4
12
20
28
36
44
Mass Number

(A) (B)

Figure 7

Figure 8. Typical post-pulse (A) and background (B) residual gas spectra for PE-16 (a high nickel stainless steel). These spectra were recorded after exposure of PE-16 samples to 30 shock tube pulses.

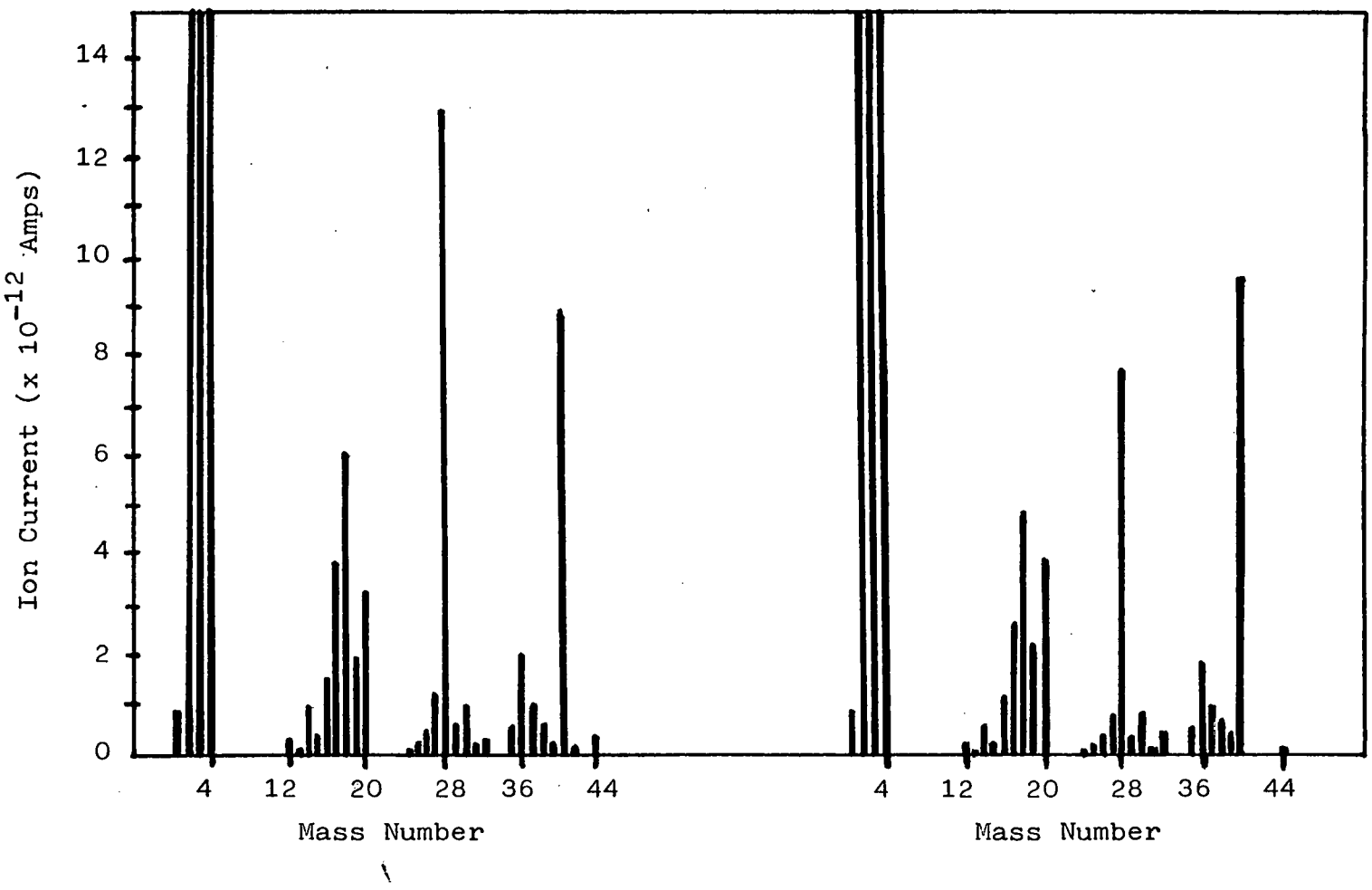
Ion Current (x 10^{-12} Amps)
0
2
4
6
8
10
12
14
4
12
20
28
36
44
Mass Number
4
12
20
28
36
44
Mass Number

(A) (B)

Figure 8

Figure 9. A plot of the CD_4 peak height (20 peak) vs. shock tube pulse number. ATJ-S graphite was bombarded for the first 200 pulses and PE-16 was bombarded for the next 50 pulses.

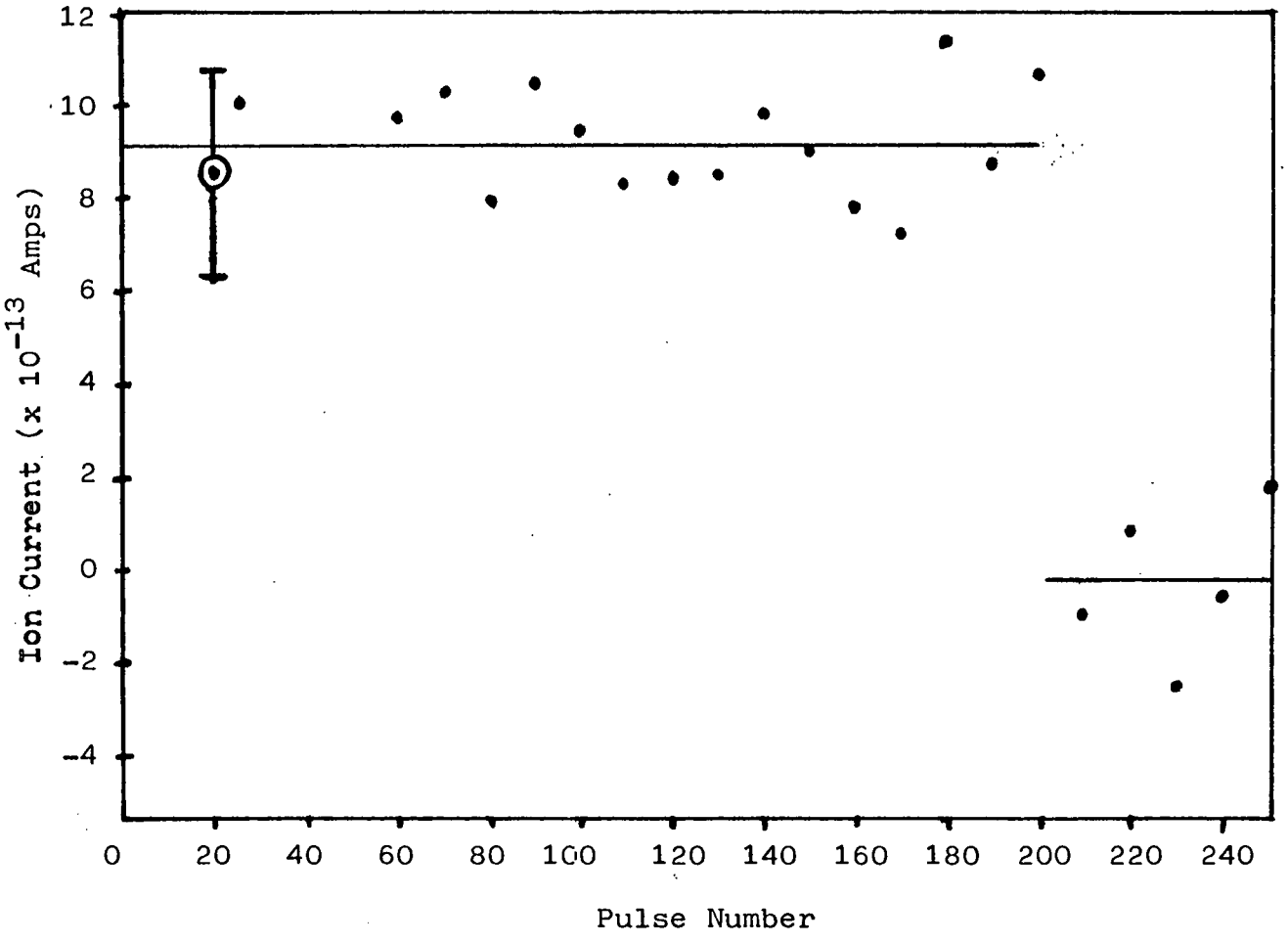
12
10
8
6
4
2
0
-2
-4
Ion Current (x 10^{-13} Amps)
0
20
40
60
80
100
120
140
160
180
200
220
240
Pulse Number

Figure 9

Figure 10. A plot of the CD_4 peak heights (16 and 18 peaks) vs. shock tube pulse number for bombardment of ATJ-S graphite.

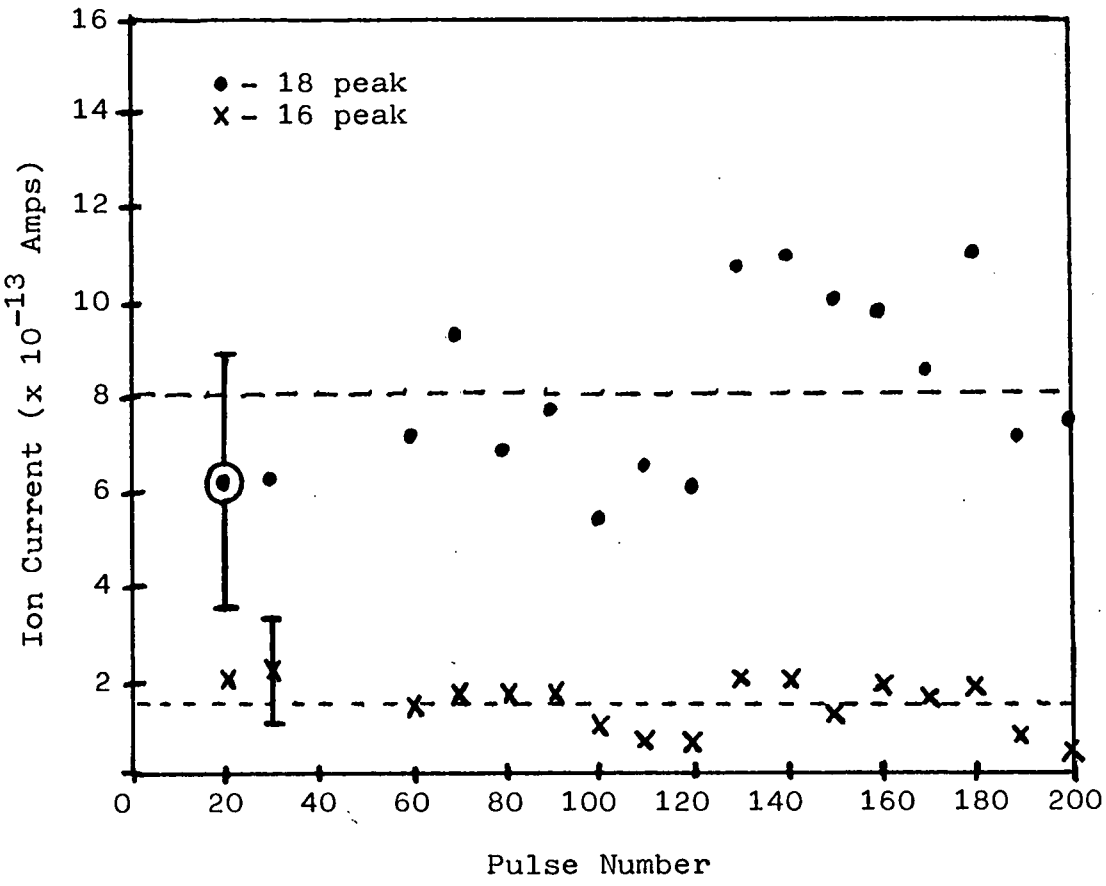
16
14
12
10
8
6
4
2
0
20
40
60
80
100
120
140
160
180
200
● - 18 peak
x - 16 peak
Ion Current (x 10^{-13} Amps)
Pulse Number

Figure 10

Figure 11. SEM micrographs of the surfaces of ATJ-S graphite samples illustrating the three distinct surface areas: dark gray areas, which represent bulk graphite; light gray areas, which represent thin layers of graphite above sub-surface pores; and pore areas.

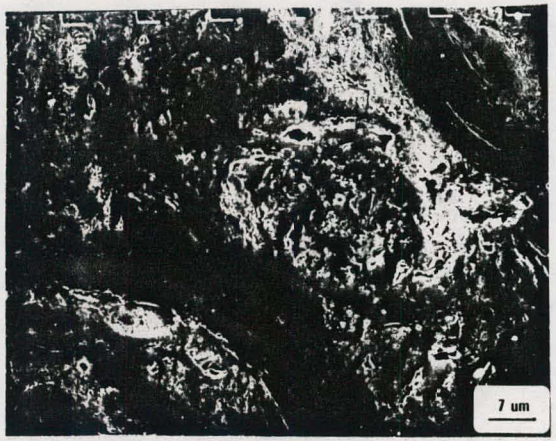

(A)

(B)

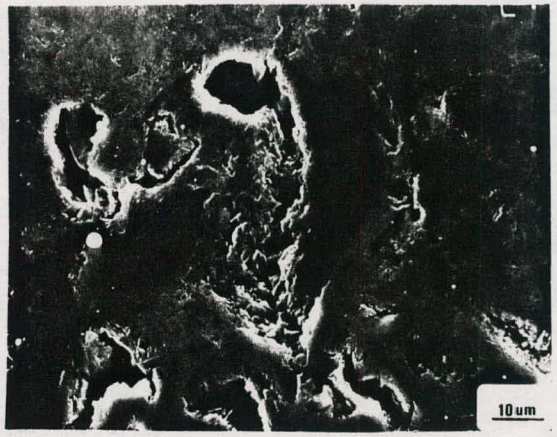

(C)

FIGURE 11

Figure 12. SEM micrographs of typical areas of the surfaces of ATJ-S graphite samples after plasma exposure for 0 (A), 40 (B), and 200 (C) shock tube pulses at a mean incident ion energy of 800 eV. Notice the increase in the number of light gray areas with exposure indicating that erosion occurred preferentially at the thin layered regions above sub-surface pores.

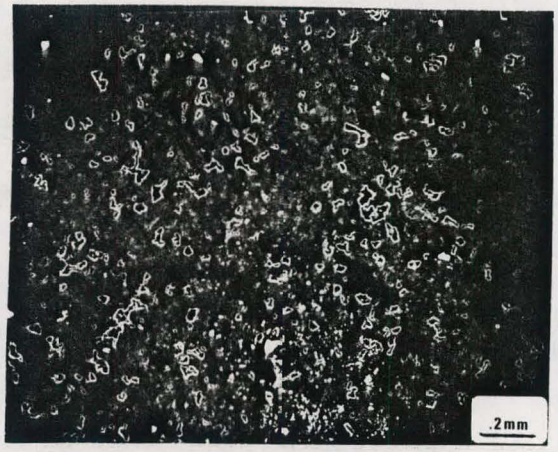

(A)

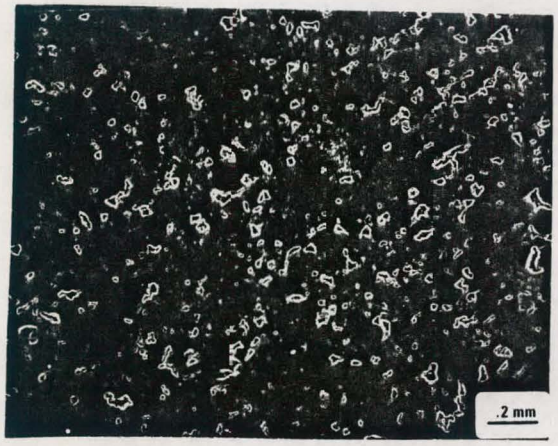

(B)

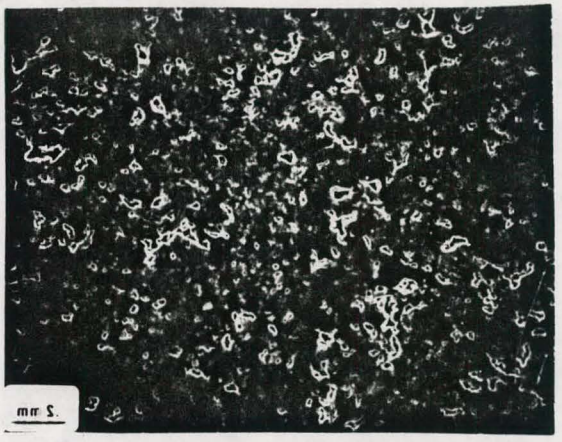

(C)

FIGURE 12

Figure 13. SEM micrographs of typical areas of the surfaces of ATJ-S graphite samples after plasma exposure for 0 (A), 40 (B), and 200 (C) shock tube pulses at a mean incident ion energy of 800 eV. Notice the increased surface erosion with plasma exposure.

(A)

(B)

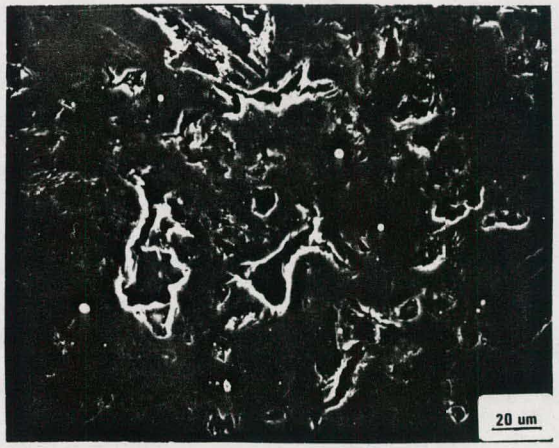

(C)

FIGURE 13

Figure 14. SEM micrographs of typical areas of the surfaces of ATJ-S graphite samples after plasma exposure for 0 (A), 40 (B), and 200 (C) shock tube pulses at a mean incident ion energy of 800 eV. Notice the increased loss of surface detail with plasma exposure.

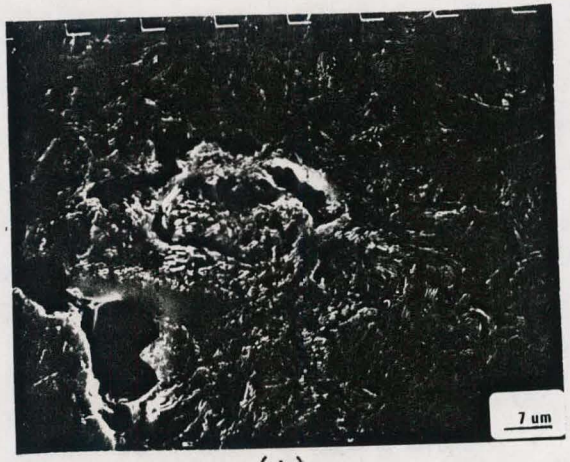

(A)

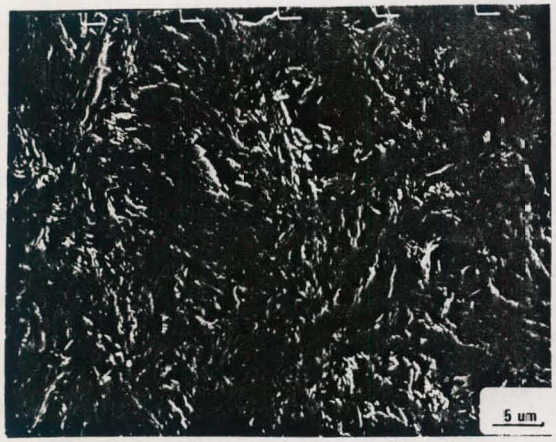

(B)

(C)

FIGURE 14

Figure 15. SEM micrographs of typical areas of the surfaces of ATJ-S graphite samples after plasma exposure for 0 (A), 40 (B), and 200 (C) shock tube pulses at a mean incident ion energy of 800 eV. Notice the increased loss of fine surface detail with plasma exposure.

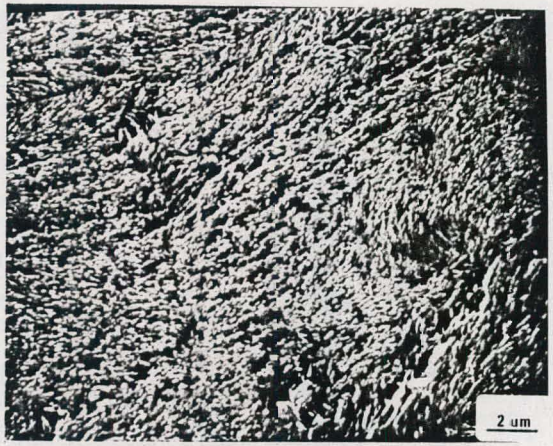

(A)

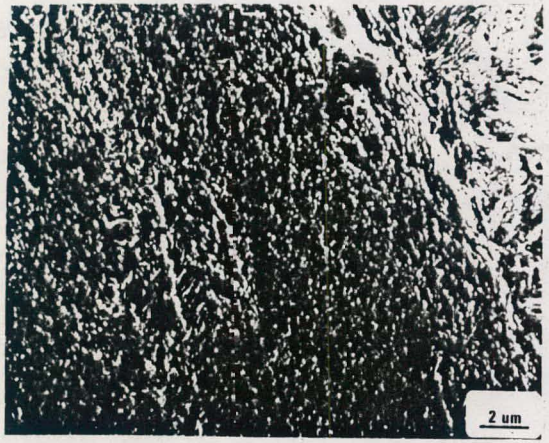

(B)

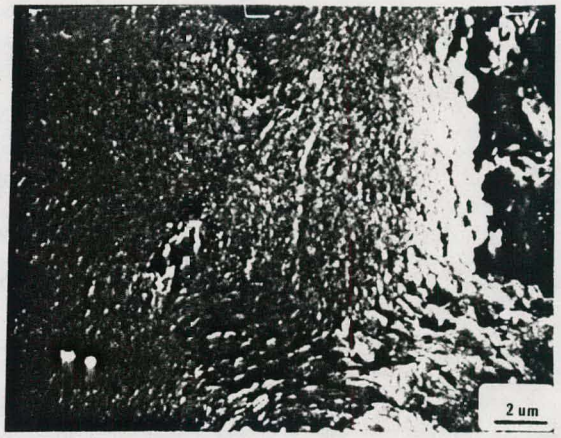

(C)

FIGURE 15

Figure 16. SEM micrographs of a flaked area on the surface of an ATJ-S graphite sample exposed for 40 pulses at an incident ion energy of 800 eV.

(A)

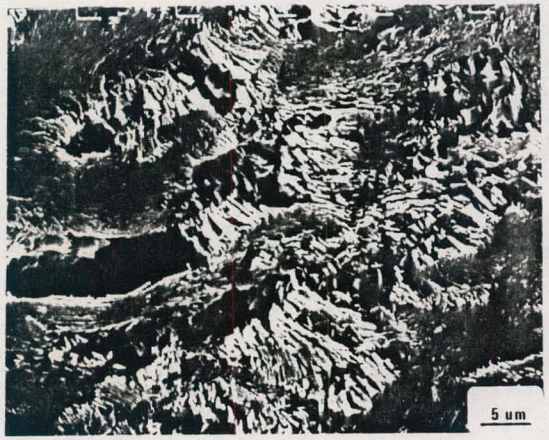

(B)

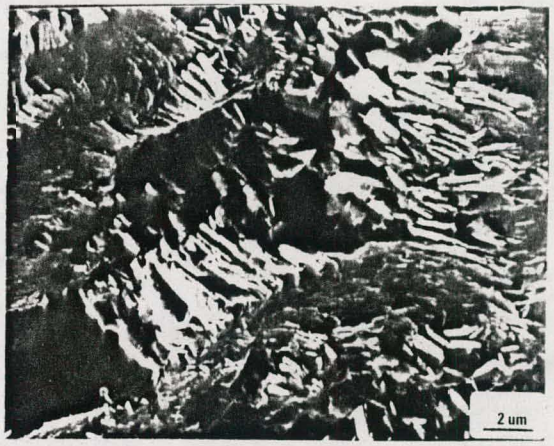

(C)

FIGURE 16

Figure 17. SEM micrographs of typical areas of the surface of ATJ-S graphite samples exposed for 44 (A) and 200 (B) pulses at a mean incident ion energy of 250 eV and for 40 (C) and 200 (D) pulses at an incident ion energy of 800 eV. Notice the increased erosion, especially at the thin layered regions, for the 800 eV cases.

(A)

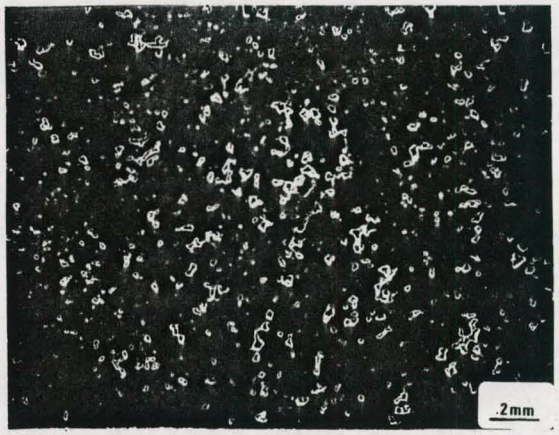

(B)

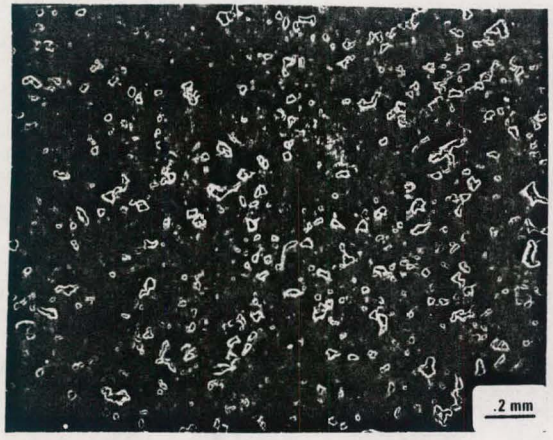

(C)

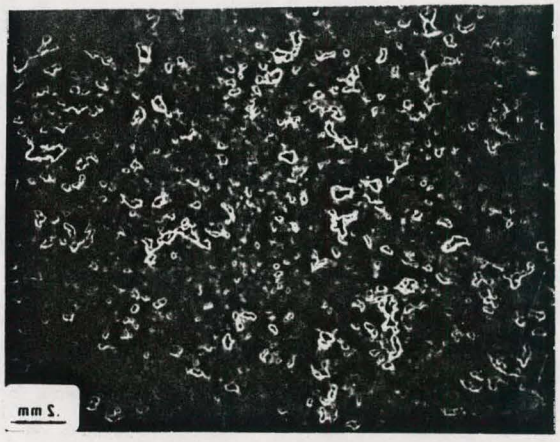

(D)

FIGURE 17

Figure 18. A schematic of the ATJ-S graphite structure near the surface showing a thin layered region above a sub-surface pore surrounded by graphite grains.

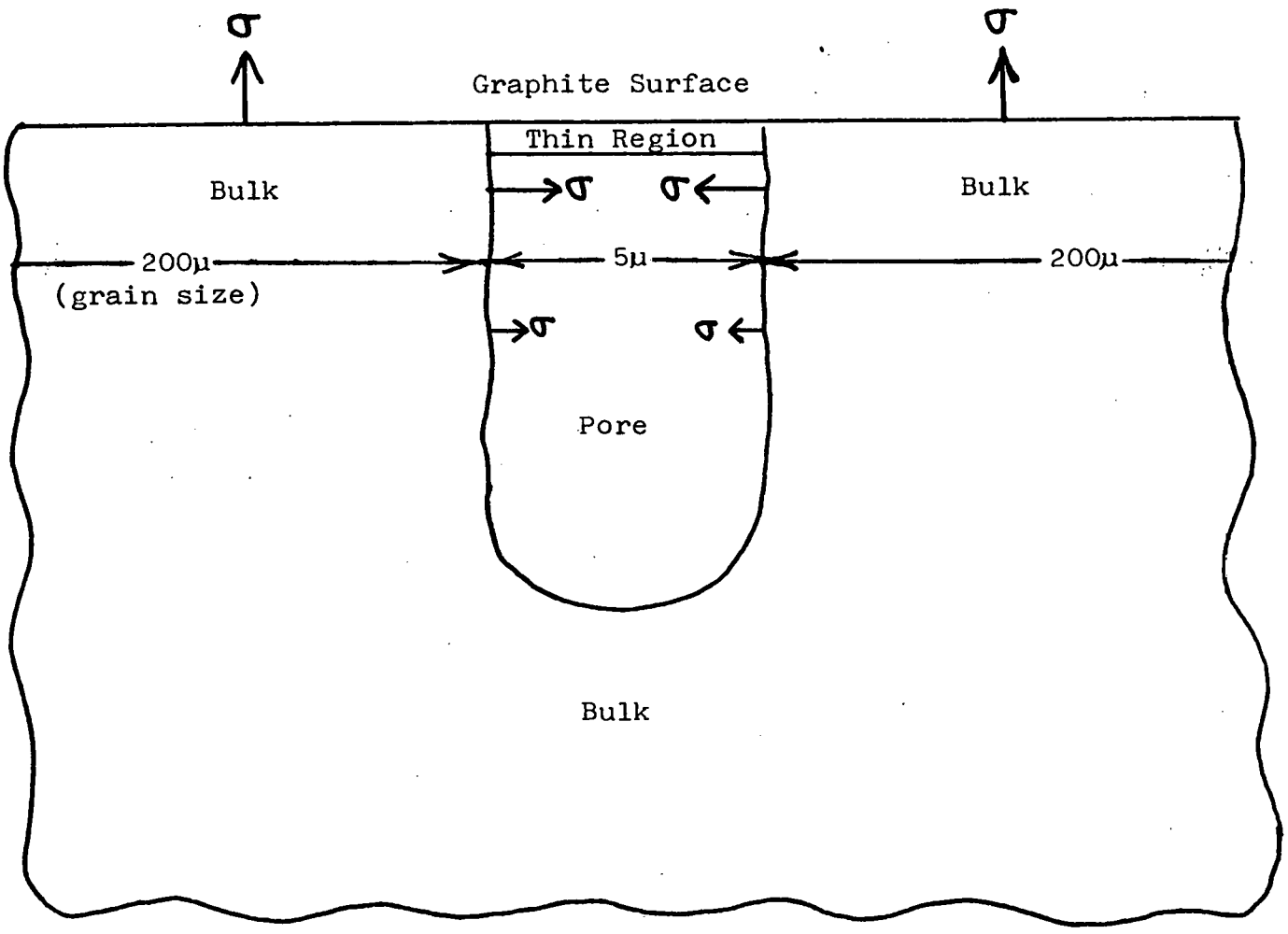
σ
σ
Graphite Surface
Thin Region
Bulk
σ
σ
Bulk
200μ
(grain size)
5μ
200μ
σ
σ
Pore
Bulk

Figure 18

TABLE 1

Summary of Previous Experimental Results for the

Impurity Production Rate of Graphite

AUTHORS	REF.	MAXIMUM IMPURITY PRODUCTION RATE (atoms/incident ion)	TYPE OF GRAPHITE	PARTICLE FLUX (sec^{-1}-m^{-2})
Thermal Particles				
Wood et.al.	12	7×10^{-4}	bulk	?
Gould	13	4×10^{-5}	?	?
Balooch et.al.	14	4.5×10^{-3}	pyrolytic	?
McCracken et.al.	15	?	?	?
Veprek et.al.	16	2×10^{-4}	pyrolytic	?
Energetic Particles				
Feinberg et.al.	17	8.5×10^{-2}	reactor	1×10^{18} H^+, 2×10^{19} H^0
Behrisch et.al.	18	2.4×10^{-2}	pyrolytic	3×10^{16} H_2^+
Roth et.al.	19	3.4×10^{-2}	pyrolytic	2×10^{16} H^+
Busharov et.al.	20	8.3×10^{-2}	?	2×10^{15} H^+
Erents et.al.	21	2.5×10^{-2}	pyrocarbon	4.6×10^{15} D^+
Sone et.al.	22	$4 \times 10^{-2}/1 \times 10^{-1}$	pyrolytic	6.3×10^{14}-2×10^{15} H^+

.....continued on next page

TABLE 1

(continued)

AUTHORS	REF.	MAXIMUM IMPURITY PRODUCTION RATE (atoms/incident ion)	TYPE OF GRAPHITE	PARTICLE FLUX (sec^{-1}-m^{-2})
Energetic Particles				
Smith et.al.	23	2×10^{-2}	thin film	6.3×10^{15} H_2^+
Branganza et.al.	24	1.5×10^{-2}	pyrocarbon	4×10^{14} D^+
Bohdansky et.al.	25	3×10^{-2}	pyrolytic	6.3×10^{15} D^+
Borders et.al.	26	5×10^{-2}	bulk	6.3×10^{14} D^+
Smith et.al.	27	1×10^{-1}	thin film	8×10^{14} H_2^+

TABLE 2

Summary of Shock Tube Plasma Characteristics

Ion Temperature	~500 eV
Ion Number Density	$\sim 10^{16}$ D^+/cm^3
Transverse Magnetic Field	~1 tesla
Ion Flux at Sample Surface	$\sim 10^{23}$ D^+/cm^2-sec
Duration of Ion Bombardment	~0.1 usec/pulse

TABLE 3

Cracking Pattern and Sensitivity Results for the

Veeco SPI-10 Residual Gas Analyzer

GAS	PEAK	PERCENTAGE OF PRIMARY PEAK	SENSITIVITY OF PRIMARY PEAK
CH_4 (CD_4)	12 (12)	3.2% $\pm$ .3%	
	13 (14)	8.8% $\pm$ .5%	
	14 (16)	18.1% $\pm$ .5%	
	15 (18)	83.3% $\pm$ .5%	
	16 (20)	100.0%	$9.8 \pm 1.0 \times 10^{-8}$ amp/Pa
N_2	14	6.2% $\pm$ .5%	
	28	100.0%	$2.3 \pm 0.1 \times 10^{-7}$ amp/Pa
H_2O	16	5.1% $\pm$ .5%	
	17	31.0% $\pm$ .5%	
	18	100.0%	———

.....continued on next page

TABLE 3
(continued)

GAS	PEAK	PERCENTAGE OF PRIMARY PEAK	SENSITIVITY OF PRIMARY PEAK
CO	12	4.9% $\pm$ .3%	
	14	1.0% $\pm$ .2%	
	16	1.6% $\pm$ .2%	
	28	100.0%	
	29	1.0% $\pm$ .2%	
	30	0.8% $\pm$ .1%	———
Ar	20	25.1% $\pm$ .5%	
	40	100.0%	$1.7 \pm 0.2 \times 10^{-7}$ amp/Pa
Trichloroethylene	35	29.4% $\pm$ .5%	
(HC_2Cl_3)	36	100.0%	
	37	9.4% $\pm$ .5%	
	38	32.1% $\pm$ .5%	———

TABLE 4

Contributions to the Residual Gas Analyzer Spectra

MASS NUMBER	CONTRIBUTIONS				MASS NUMBER	CONTRIBUTIONS			
1	H				26	C_2H_2			C_2D
2	H_2	D			27	C_2H_3			
3	HD				28	C_2H_4	N_2	CO	C_2D_2
4		D_2			29	C_2H_5			
5					30	C_2H_6	C_2H_4D		
6					31		C_2H_5D		
7					32	O_2			
8					33				
9					34				
10					35	Cl^{35}			
11					36	HCl^{35}			
12	C			C	37	DCl^{35}	Cl^{37}		
13	CH				38		HCl^{37}		
14	CH_2	N		CD	39		DCl^{37}		
15	CH_3				40	Ar			
16	CH_4	O		CD_2	41				
17		HO			42				
18		H_2O	DO	CD_3	43				
19		HDO			44	CO_2			
20			Ar	CD_4	45				
21					46				
22					47				
23					48				
24	C_2			C_2	49				
25	C_2H_1				50				

TABLE 5

Comparison of Experimental Results

with CD_4 Cracking Pattern

PEAK RATIO	EXPERIMENTAL RESULTS	CD_4 RESULTS
12/20	———	3.2%
14/20	———	8.8%
16/20	15.6%	18.1%
18/20	87.7%	83.3%
20/20	100.0%	100.0%

APPENDIX

The results of Jensen et. al.[7] show that for a 10 keV plasma, the maximum allowed impurity concentration of carbon atoms is $\sim$10%. Above this value, fusion ignition cannot occur. For a tokamak fusion reactor with a plasma number density, n_o, of $\sim 10^{20}$ particles/m^3, this implies that the maximum allowed number density of carbon atoms, n_c^{max}, is $\sim 10^{19}$ carbon atoms/m^3.

If the number of impurity molecules formed as a result of plasma bombardment correlates with the incident ion flux, ATJ-S graphite can be easily evaluated as a possible fusion reactor material by first using the impurity production rate found in this experiment to determine the number density of carbon atoms, n_c, that one would expect to find in a tokamak under actual steady-state conditions and then comparing this value of n_c to n_c^{max}. This analysis is given below.

When correlation exists, the number of carbon impurity atoms produced by plasma bombardment of graphite in a fusion reactor, N_c, is given by the following expression:

$$N_c = S\emptyset A t_o \qquad (6)$$

where S is the impurity production rate, $\emptyset$ is the particle flux to the graphite surface, A is the area of the graphite

surface exposed to the plasma, and t_o is the time of plasma bombardment. The number density, n_c, of carbon atoms is simply:

$$n_c = \frac{N_c}{V} \tag{7}$$

where V is the volume occupied by the plasma. We now have the following expression for n_c:

$$n_c = \frac{S\phi A t_o}{V} \tag{8}$$

This expression must now be evaluated using typical values for the various parameters. The plasma volume, V, in a tokamak reactor is typically $\sim$500 m^3 and the impurity production rate, S, found in this investigation is 18 carbon atoms/incident ion. The plasma bombardment time, t_o, should be the minimum plasma energy confinement time for fusion ignition. For a 10 keV plasma, Lawson's criteria indicates that nt must be greater than $\sim 4 \times 10^{20}$ sec/m^3.[6,7] Using the plasma number density, n_o, of $\sim 10^{20}$ particles/m^3, the energy confinement time is then $\sim$10 sec. This gives us the following expression for n_c:

$$n_c = 3.6 \times 10^{-1}\ \phi A\ \frac{\text{carbon}}{D^+}\ \frac{\text{sec}}{m^3} \tag{9}$$

Since ATJ-S graphite is being strongly considered for use as a limiter material, ϕ and A must be evaluated for the limiter position. A typical limiter geometry in present experimental tokamak devices is the rail geometry. Charged particles travel in the direction of the magnetic field lines in the torus and strike the face of the limiter that is perpendicular to the field lines. The particle flux at the limiter can be computed using the following expression based on simple kinetic theory:

$$\phi_{limiter} \simeq \frac{\bar{n}_{edge} \cdot \bar{c}}{4} \qquad (10)$$

where $\bar{n}_{edge}$ is the mean number density at the plasma edge and $\bar{c}$ is the mean particle velocity at the plasma edge. Assuming that $\bar{n}_{edge}$ is $\sim \frac{n}{100}$ and the mean particle energy is $\sim$ 500 eV, we have that

$$\phi_{limiter} \simeq 5 \times 10^{22} D^+/m^2\text{-sec} \qquad (11)$$

However, this is only for the leading edge of the limiter. The particle flux decreases with distance from the leading edge. In this analysis, we assume that the particle flux, $\phi_{limiter}$, decreases exponentially with x, the distance from the leading edge, and is given by:

$$\underset{\text{limiter}}{\phi(x)} = 5 \times 10^{22} \frac{D^+}{m^2\text{-sec}} \exp(-x/a) \qquad (12)$$

where a is the characteristic length. For a typical rail limiter of 1 cm thickness, a is assumed to be .25 cm. Hence we have

$$\underset{\text{limiter}}{\phi(x)} = 5 \times 10^{22} \frac{D^+}{m^2\text{-sec}} \exp(-x/.25) \qquad (13)$$

Since ϕ_{limiter} now varies over the face of the limiter surface exposed to the plasma the product $\phi_{\text{limiter}} \cdot A$ must be replaced with the integral, $\int_{\text{limiter}} \phi(A) \cdot dA$. But dA is just $\ell \cdot dx$ where ℓ is the limiter length which is typically 10 cm. So, we then have

$$\int_{\substack{\text{limiter} \\ \text{surface}}} \underset{\text{lim.}}{\phi(x)} dA = \int_{x=0}^{x=1} \underset{\text{lim.}}{\phi(x)} \ell dx = 5 \times 10^{19} \frac{D'}{m\text{-sec}} \int_{x=0}^{x=1} \exp(x/.25)dx \qquad (14)$$

Evaluating this expression, we find that

$$\int_{\substack{\text{limiter} \\ \text{surface}}} \phi(x)dA \simeq 1.2 \times 10^{19} \frac{D^+}{\text{sec}} \qquad (15)$$

Upon substituting this for $\emptyset \cdot A$ in equation (9), we find that

$$n_c \simeq 4 \times 10^{18} \text{ carbon atoms/m}^3 \qquad (16)$$

Since we have that $n_c^{max} \simeq 1 \times 10^{19}$ carbon atoms/m^3 for $n_o \simeq 1 \times 10^{20}$ particles/m^3, we see that

$$n_c \simeq n_c^{max} \qquad (17)$$

This analysis shows that the impurity concentration of carbon atoms is close to the critical impurity concentration. It must be pointed out that this analysis only gives a very rough estimate for n_c. The mean plasma number density and the mean ion energy at the plasma edge are not well known at present. The value of the mean ion energy used in this analysis, 500 eV, is thought to be reasonable and typical for a tokamak reactor. The variation of ion flux across the limiter surface is not well known. Also, this estimate is only for one limiter; whereas, tokamak reactors will employ several sets of limiters. In addition, this estimate assumes that all carbon atoms leaving the surface of the limiter enter the plasma, which is unlikely. As plasma conditions at the limiter become better known and limiter designs change, this value for n_c will change. However, on the basis of this analysis, we may conclude that at the present time, impurity production is a seri-